NJC

PAPER

View Article Online
View Journal | View Issue

Published on 11 January 2018. Downloaded by National Library of Serbia on 5/30/2020 12:11:45 PM.

Check for updates

Cite this: *New J. Chem.*, 2018, **42**, 3001

Ruthenium–arene complexes with NSAIDs: synthesis, characterization and bioactivity†

Ana Tadić,[a] Jelena Poljarević,*[a] Milena Krstić,[b] Marijana Kajzerberger,[c] Sandra Aranđelović,[c] Siniša Radulović,[c] Chrisoula Kakoulidou,[d] Athanasios N. Papadopoulos,[e] George Psomas[d] and Sanja Grgurić-Šipka*[a]

Two non-steroidal antiinflammatory drugs indomethacin and mefenamic acid were coordinated to Ru(II)–arenes to afford four new complexes. The cytotoxic activities of the ligands and ruthenium complexes were tested in three human cancer cell lines (K562, A549, MDA-MB-231) and non-tumour human fetal lung fibroblast cells (MRC-5) by MTT assay. Cytotoxicity studies revealed that indomethacin Ru(II)–arene complexes **1** and **3** displayed good cytotoxicity and apparent cytoselective profiles. The IC_{50} values obtained in leukemia K562 cells were comparable to those of cisplatin (10.3 μM (CDDP), 11.9 μM (**1**) and 13.2 μM (**3**)). Flow cytometric analysis of **1** and **3** in triple-negative breast cancer MDA-MB-231 cells revealed an interesting mechanism of action. At IC_{50} concentrations, **1** and **3** arrested cell cycle progression in S phase and caused rapid accumulation of cells in sub-G1 phase (up to 48%), while Annexin V-FITC/PI staining showed simultaneous occurrence of apoptotic and necrotic cell populations at approximately similar levels of 20%. Measurement of reactive oxygen species (ROS) production by DCFH-DA staining confirmed the potential of **1** and **3** to increase ROS even more than cisplatin. The interaction of the complexes with serum albumins showed their potential ability to bind tightly and reversibly to albumins. The affinity of the complexes to calf-thymus DNA was investigated by UV-vis spectroscopy, viscosity measurements and fluorescence emission spectroscopy for competitive studies of the complexes with ethidium bromide, revealing that their interaction probably occurs *via* intercalation. Taken together, the results strongly suggest the potential of complexes **1** and **3** to alter cell cycle progression and cause DNA-damage by means of direct DNA-binding or indirectly by ROS production.

Received 13th November 2017,
Accepted 10th January 2018

DOI: 10.1039/c7nj04416j

rsc.li/njc

Introduction

Rosenberg's highly significant discovery of cisplatin[1] opened the way for the introduction of metal complexes in cancer chemotherapy; since then, scientists have been searching for new potential anticancer compounds. Currently, research in that field is focused on ruthenium(II) complexes.[2] Ruthenium complexes have been investigated for use as DNA topoisomerase inhibitors,[3] TrxR inhibitors,[4] antimicrobial agents,[5] molecular probes[6] and anticancer agents.[7] Also, ruthenium can mimic iron in binding with certain biological molecules, particularly transferrin, and Ru(II) and Ru(III) complexes can display similar ligand exchange kinetics to Pt(II).[8] Considering all these characteristics, ruthenium complexes are suitable for medical applications. Three of these, namely KP1339, KP1019 and NAMI, have entered clinical trials, with promising results.[2,9,10] A number of ruthenium(II) complexes bearing π-bonded arene ligands have already been developed and have shown promising anticancer activities.[11] Because the concentration of oxygen in tumor cells is low, the environment is more reductive than in normal tissue, favouring the active reduced form.[8,12]

A real revolution in medicine occurred with the discovery of non-steroidal anti-inflammatory drugs (NSAIDs), which have been proven to be biologically active compounds. NSAIDs are one of the most commonly used classes of medication.[13] Their main mechanism of action is based on the inhibition of the enzyme cyclooxygenase (COX), more precisely, its two isoforms: COX-1 and COX-2. By this method, they prevent the formation of various prostaglandins responsible for the physiological responses of fever, pain sensation and anti-inflammation.[14] Also, NSAIDs have synergistic action on the activity of certain

[a] *University of Belgrade – Faculty of Chemistry, Studentski trg 12-16, 11000 Belgrade, Serbia. E-mail: sanjag@chem.bg.ac.rs, jelenal@chem.bg.ac.rs*
[b] *Faculty of Veterinary Medicine, University of Belgrade, Bulevar oslobodjenja 18, 11000 Belgrade, Serbia*
[c] *Institute for Oncology and Radiology of Serbia, Pasterova 14, 11000 Belgrade, Serbia*
[d] *Department of General and Inorganic Chemistry, Faculty of Chemistry, Aristotle University of Thessaloniki, P.O. Box 135, GR-54124 Thessaloniki, Greece*
[e] *Department of Nutrition and Dietetics, Faculty of Food Technology and Nutrition, Alexandrion Technological Educational Institution, Sindos, Thessaloniki, Greece*

† Electronic supplementary information (ESI) available. See DOI: 10.1039/c7nj04416j

Published on 11 January 2018. Downloaded by National Library of Serbia on 5/30/2020 12:11:45 PM.

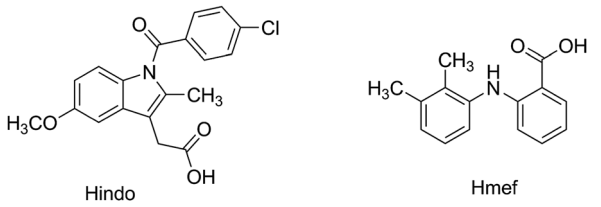

Fig. 1 Structure formulas of the NSAIDs Hindo and Hmef.

antitumor drugs[15] and can lead to cell death of a series of cancer cell lines *via* apoptosis.[16] Metal complexes containing NSAIDs[17] are among the compounds which have received much attention and increasing interest from a medicinal inorganic chemistry viewpoint because they are found in coordination compounds which have active drugs as ligands.[15]

Indomethacin (Hindo, Fig. 1) is a phenylalkanoic acid and is one of the most potent clinically used NSAIDs. It is used to relive pain, fever and inflammation. Despite the known adverse gastrointestinal side-effects (ulceration and hemorrhage) limiting the doses and use of NSAIDs, Hindo and its Cu(II) complex are widely safely administered in the clinical treatment of acute inflammation and other medical conditions in humans.[18] A series of copper(II)[19–22] and two tin[23] complexes with indomethacin as a ligand have been reported in the literature.

Mefenamic acid (Hmef, Fig. 1), or *N*-phenylanthranilic acid, is in clinical use. Mefenamic acid is an effective analgesic and antipyretic agent with relatively mild side-effects, including headaches, diarrhea, vomiting and nervousness.[24,25] Recently, Cu(II),[26–29] Co(II),[30,31] Ni(II),[32] Zn(II),[33] Mn(II)[34] and Sn(IV)[35] complexes with mefenamato ligands have been reported.

Recently, Hartinger and Dyson showed in separate studies that oxicam-based NSAIDs, as well as aspirin, coordinate to Ru(II) and Os(II) ions in half-sandwich complexes, providing antitumor-active compounds.[36–39] Based on these results, the aim of our work presented here was to combine two well-known drugs (NSAIDs) with Ru(II)–arene precursors in order to obtain new half-sandwich Ru(II)–arene complexes with improved cytotoxic activities. This may be a method to alter the purpose of these drugs and to obtain potentially good cytotoxic agents. We synthesized four new complexes and completely characterized them. Furthermore, we investigated their cytotoxic activities by MTT assay. In order to explain the cytotoxicity results, we have analyzed the cell cycle, using flow-cytometric analysis and the annexin V-FITC apoptotic assay, for quantitative analysis of apoptotic and necrotic death of selected cells. We have also measured the production of intracellular reactive oxygen species (ROS) and tested the ability of the compounds to scavenge 1,1-diphenyl-picrylhydrazyl (DPPH), hydroxyl radicals ($^{\bullet}$OH) and 2,2′-azinobis-(3-ethylbenzothiazoline-6-sulfonic acid) (ABTS) radicals and to inhibit soybean lipoxygenase (LOX) activity. Additionally, we examined the *in vitro* affinity of the complexes for bovine serum albumin (BSA) and human serum albumin (HSA) by fluorescence emission spectroscopy as well as the *in vitro* interaction of the complexes with calf-thymus (CT) DNA by UV-vis spectroscopy, viscosity measurements and fluorescence emission spectroscopy.

Experimental section

Materials and measurements

$RuCl_3{\cdot}3H_2O$ was purchased from Johnson Matthey (London, UK). Indomethacin and mefenamic acid were purchased from TCI (Tokyo, Japan). Trisodium citrate, NaCl, CT DNA, BSA, HSA, EB, DPPH, ABTS, sodium linoleate, butylated hydroxytoluene (BHT), 6-hydroxy-2,5,7,8-tetramethylchromane-2-carboxylic acid (trolox), nordihydroguaiaretic acid (NDGA) and caffeic acid were purchased from Sigma-Aldrich. $[Ru(\eta^6\text{-}p\text{-cymene})Cl_2]_2$ was prepared according to a published procedure.[40] $[Ru(\eta^6\text{-toluene})Cl_2]_2$ was prepared according to a published procedure.[41] Solvents were obtained and used without further purification. Infrared spectra were recorded on a Nicolet 6700 FTIR spectrometer using the ATR technique. NMR spectra were recorded on a Bruker Avance III 500 MHz spectrometer. Chemical shifts for ^{1}H and ^{13}C NMR spectra were referenced to residual ^{1}H and ^{13}C present in $CDCl_3$ or DMSO-d_6. ESI mass spectra of the ruthenium complexes were recorded on a 6210 Time-of-Flight LC-MS instrument (G1969A, Agilent Technologies) in both positive and negative ion modes using CH_3CN/H_2O or CH_3CN as solvents. UV-vis spectra were recorded in solution at concentrations in the range of 10^{-5}–10^{-3} M on a Hitachi U-2001 dual beam spectrophotometer. Fluorescence spectra were recorded in solution on a Hitachi F-7000 fluorescence spectrophotometer. Viscosity experiments were carried out using an ALPHA L Fungilab rotational viscometer equipped with an 18 mL LCP spindle.

DNA stock solution was prepared by dilution of CT DNA with buffer (containing 150 mM NaCl and 15 mM trisodium citrate at pH 7.0) followed by vigorous stirring at 4 °C for three days; the solutions were maintained at 4 °C for no longer than two weeks. The stock solution of CT DNA gave a ratio of UV absorbance at 260 and 280 nm (A_{260}/A_{280}) in the range of 1.85 to 1.90, indicating that the DNA was sufficiently free of protein contamination.[42] The concentration of CT DNA was determined by the UV absorbance at 260 nm after 1 : 20 dilution using ε = 6600 M^{-1} cm^{-1}.[43]

Synthesis of the complexes

Synthesis of K[Ru(η^6-*p*-cymene)(indo)Cl_2], 1. A solution of Hindo (0.0584 g, 0.163 mmol) in ethanol (5 mL) was neutralized with potassium hydroxide (9.13 mg, 0.163 mmol) and stirred for 1 h at room temperature. After that, a suspension of $[Ru(\eta^6\text{-}p\text{-cymene})Cl_2]_2$ (0.05 g, 0.08 mmol) in ethanol (5 mL) was added to the ligand solution, and the reaction mixture was precipitated. The precipitate was filtered and dried *in vacuo*. Yield: 62 mg, 54%. Anal. calc. for $C_{29}H_{29}Cl_3NO_4RuK$: C, 49.60; H, 4.13; N, 1.99. Found: C, 49.73; H, 4.21; N, 2.09. δ (ppm) H (500 MHz; $CDCl_3$): 1.31 ($CH(C\boldsymbol{H}_3)_2$, 6H), 2.19 (CH_3 cymene, C11, C6 7H), 2.28 ($C\boldsymbol{H}(CH_3)_2$, 1H), 3.43 (C9, 2H), 3.85 (C19, 3H), 5.34 (C2, C6, cym, 2H), 5.57 (C3, C5, cym, 2H), 6.64 (C3, 1H), 6.87 (C1, 1H), 6.97 (C4, 1H), 7.46 (C15, C17, 2H), 7.63 (C14, C18, 2H). δ (ppm) C (125 MHz; DMSO-d_6): 13.49 (C11), 19.03 ($\mathbf{C}H(CH_3)_2$), 22.82 ($CH(\mathbf{C}H_3)_2$), 31.61 (C6, $\mathbf{C}H(CH_3)_2$), 56.08 (C19), 94.49 (C3, C5 cym), 100.21 (C2, C6 cym), 101.62 (C1 cym, C4 cym), 112.09 (C1), 112.26 (C3), 114.83 (C4, C7),

 This journal is © The Royal Society of Chemistry and the Centre National de la Recherche Scientifique 2018

Published on 11 January 2018. Downloaded by National Library of Serbia on 5/30/2020 12:11:45 PM.

129.11 (C5), 131.28 (C15, C17), 134.30 (C13), 135.62 (C14, C18), 139.24 (C8, C16), 156.01 (C2), 168.60 (C10, C12). IR (ATR), ν_{max}/cm^{-1}: 2963 (C–H), 1686 (C═O), 1453 (C–C_{ar}), 1261 (C–O_v), 1226 (C–H_δ), 841 (C–H_γ). LC-ESI/MS, *m*/*z* (M, %): 592.08 ($[M - K - 2Cl]^+$, 18), 633.11 ($[M - K - Cl + H]^+$, 45).

Synthesis of $(NH_4)[Ru(\eta^6$-*p*-cymene)(mef)$Cl_2]$, 2. A suspension of Hmef (0.04 g, 0.163 mmol) in methanol (5 mL) was added to a suspension of $[Ru(\eta^6$-*p*-cymene)$Cl_2]_2$ in methanol (5 mL). The reaction mixture was stirred at room temperature for 1 h. The orange suspension was than concentrated *in vacuo* to 5 mL, and solid NH_4PF_6 (0.03 g) was added. The mixture was stirred at room temperature for 2 h. The resulting orange precipitate was filtered and dried *in vacuo*. Yield: 51 mg, 55%. Anal. calc. for $C_{25}H_{32}Cl_2N_2O_2Ru$: C, 53.18; H, 5.67; N, 4.96. Found: C, 53.60; H, 5.69; N, 4.53. δ (ppm) H (500 MHz; DMSO-d_6): 1.20 (CH(C***H***$_3)_2$, 6H), 2.10 (C14, 3H; CH_3 cym, 3H), 2.29 (C15, 3H), 2.86 (C***H***$(CH_3)_2$, 1H), 5.78 (C2, C6, cymene 2H), 5.90–6.10 (C3, C5 cymene 2H), 6.69 (C11, C13) 7.03–7.13 (C12, C4, C5), 7.31 (C3, 1H), 7.88 (C6, 1H), 9.44 (NH). δ (ppm) C (125 MHz; DMSO-d_6): 13.43 (C15), 18.12 (CH_3), 19.76 (C14), 21.41 (CH(***C***$H_3)_2$), 29.61 (***C***$H(CH_3)_2$), 85.37 (C3 cym), 86.41 (C5 cym), 89.31 (C2 cym), 95.33 (C6 cym) 100.03 (C4 cym), 106.36 (C1 cym), 111.20 (C6), 112.92 (C2), 116.15 (C4), 122.32 (C11), 126.02 (C12), 126.41 (C13), 131.10 (C3), 131.57 (C9), 134.19 (C5), 137.87 (C10), 138.28 (C8), 148.56 (C7), 169.97 (C1). IR (ATR), ν_{max}/cm^{-1}: 3309 (N–H_v), 2975–2871 (C–H_v), 1649 (C═O_v), 1497 (C–C_{ar}), 1257 (C–O_v), 1159 and 1054 (C–H_δ), 835 (C–H_γ). LC-ESI/MS, *m*/*z* (M, %): 432.24 ($[M - NH_4 - 2Cl - CH(CH_3)_2]^+$, 8), 476.12 ($[M - NH_4 - 2Cl]^+$, 10), 576.94 ($[M + CH_3OH]^+$, 100).

Synthesis of $K[Ru(\eta^6$-*p*-toluene)(indo)$Cl_2]$, 3. The synthesis of complex **3** is the same as for complex **1** with the use of $[Ru(\eta^6$-toluene)$Cl_2]_2$ instead of $[Ru(\eta^6$-*p*-cymene)$Cl_2]_2$. The resulting orange precipitate was filtered and dried *in vacuo*. Yield: 70 mg, 65%. Anal. calc. for $C_{26}H_{22}Cl_3NO_4RuK{\cdot}CH_3OH$: C, 46.90; H, 3.76; N, 2.03. Found: C, 46.60; H, 3.61; N, 2.09. δ (ppm) H (500 MHz; DMSO-d_6): 2.07 (C11, 3H), 2.14 (CH_3 tol, 3H), 3.52 (C9, 1H), 3.72 (C19, 1H), 5.71 (C2, C4, C6, tol 3H), 5.98 (C3, C5, tol 2H), 6.71 (C3, 1H), 6.96 (C1, 1H), 7.23 (C4, C15, 2H), 7.65 (C14, C17, C18, 3H). δ (ppm) C (125 MHz; DMSO-d_6): 13.94 (C11), 19.24 (C7 tol), 33.19 (C9), 55.91 (C19), 82.60 (C4 tol), 85.03 (C3, C5 tol), 89.77 (C2, C6 tol), 102.19 (C1), 105.87 (C1 tol), 111.48 (C3), 113.76 (C4), 114.91 (C7), 126.10 (C5) 128.59 (C15), 129.39–131.46 (C14, C17, C18), 134.22 (C6, C13), 137.95 (C8, C16), 155.86 (C2), 168.06 (C12), 182.97 (C10). IR (ATR), ν_{max}/cm^{-1}: 2972 (C–H_v), 1648 (C═O_v), 1447 (C–C_{ar}), 1257 (C–O_v), 1158 (C–H_δ), 835.50 (C–H_γ). LC-ESI/MS, *m*/*z* (M, %): negative mode 621.97 ($[M - K^+]^-$, 25), positive mode 623.97 ($[M - K^+ + 2H]^+$, 15), 550.04 ($[M - K^+ - 2Cl + H]^+$, 10).

Synthesis of $(NH_4)[Ru(\eta^6$-*p*-toluene)(mef)$Cl_2]$, 4. The synthesis of complex **4** is the same as for complex **2** with the use of $[Ru(\eta^6$-toluene)$Cl_2]_2$ instead of $[Ru(\eta^6$-*p*-cymene)$Cl_2]_2$. The resulting yellow precipitate was filtered and dried *in vacuo*. Yield: 32.2 mg, 54.12%. Anal. calc. for $C_{22}H_{25}Cl_2N_2O_2Ru{\cdot}2CH_3OH$: C, 49.22; H, 5.45; N, 4.78. Found: C, 49.68; H, 5.13; N, 4.38. δ (ppm) H (500 MHz; DMSO-d_6): 2.10 (C14, 3H), 2.30 (CH_3 tol, 3H), 5.71 (C2,4,6 tol, 3H), 5.97 (C3,5 tol, 2H), 6.67–6.69 (C11, C13, 2H), 7.11–7.19 (C12, C4, C5, C3 4H), 7.90 (C6, 1H), 9.46 (NH). δ (ppm) C (125 MHz; DMSO-d_6): 13.87 (CH_3 tol), 20.43 (C15), 21.23 (C14), 82.36 (C4 tol), 85.15 (C3, C5 tol), 89.94 (C2, C6 tol), 111.46 (C1 tol, C6), 111.76 (C2), 113.55 (C4), 116.69 (11), 122.22 (C12), 125.32 (C13), 128.44 (C3), 131.14 (C9), 131.96 (C5), 134.55 (C10), 138.57 (C8), 148.81 (C7), 170.62 (C1). IR (ATR), ν_{max}/cm^{-1}: 3309 (N–H_v), 3085 (C–H_v), 1649 (C═O_v), 1449 (C–C_{ar}), 1253 (C–O_v), 1157 (C–H_δ), 829 (C–H_γ). LC-ESI/MS, *m*/*z* (M, %): 541.98 ($[M + NH_4]^+$, 25), 432.13 ($[M - NH_4 - 2Cl]^+$, 10).

Cell lines and culture conditions

K562 (human myelogenous leukemia), A549 (human lung adenocarcinoma) and MRC-5 (non-tumor human lung fibroblast) cells were maintained in Roswell Park Memorial Institute (RPMI) 1640 nutrient medium (Sigma-Aldrich Co). MDA-MB-231 (human breast adenocarcinoma) cells were maintained in Dulbecco's modified Eagle's medium (DMEM) (Sigma-Aldrich Co). RPMI 1640 nutrient medium was prepared in sterile ionized water and supplemented with penicillin (192 U mL^{-1}), streptomycin (200 μg mL^{-1}), 4-(2-hydroxyethyl) piperazine-1-ethanesulfonic acid (HEPES) (25 mM), L-glutamine (3 mM) and 10% heat-inactivated fetal calf serum (FCS) (pH 7.2). To maintain the MDA-MB-231 cell line, DMEM was additionally supplemented with D-glucose (4.5 g L^{-1}). Cells were maintained as monolayer cultures in tissue culture flasks (Thermo Scientific Nunc™) in an incubator at 37 °C in a humidified air atmosphere composed of 5% CO_2.

MTT assay

The cytotoxicities of the investigated ruthenium(II) compounds and CDDP (*cis*-diamminedichloridoplatinum(II), cisplatin)[44] as a reference compound were determined using the 3-(4,5-dimethylthiazol-yl)-2,5-diphenyltetrazolium bromide (MTT, Sigma-Aldrich Co) assay.[45] Cells were seeded into 96-well culture plates (Thermo Scientific Nunc™). Due to the different morphological and physiological features of the different cell lines, cells were seeded at cell densities of 6000 c/w (K562), 7000 c/w (A549 and MDA-MB-231) and 8000 c/w (MRC-5) in 100 μL of culture medium. 24 h after seeding, the cells were exposed to serial dilutions of the tested compounds. Stock solutions of the investigated compounds were prepared by dissolving each compound in dimethyl sulfoxide (DMSO) at a concentration of 10 mM (the final concentration of DMSO did not exceed 1% per well) immediately prior to use,[46] followed by dilution with nutrient medium to the desired final concentrations (in the range of 0 to 300 μM). The stabilities of the complexes in DMSO/phosphate buffer (pH 7.4) = 1/100 (volume ratio) were monitored by UV-vis spectroscopy, and their stabilities under these conditions were proved.

Each concentration was tested in triplicate. After 72 h of continuous drug incubation, 20 μL of MTT solution (5 mg mL^{-1} in phosphate buffer solution (PBS), pH 7.2), was added to each well. Samples were incubated for the next 4 h at 37 °C with 5% CO_2 in a humidified air atmosphere. The purple formazan products were dissolved in 100 μL of 10% sodium dodecyl sulfate (SDS). Absorbances were recorded after 24 h on a microplate reader (Thermo Labsystems Multiskan EX 200-240V) at a

Published on 11 January 2018. Downloaded by National Library of Serbia on 5/30/2020 12:11:45 PM.

wavelength of 570 nm. The IC_{50} values (concentration of investigated agent that decreases the number of viable cells by 50% in a treated cell population compared to a non-treated control) were estimated from the dose–response curves.

Cell cycle analysis

Flow-cytometric analysis of the cell cycle phase distribution was performed in MDA-MB-231 cells after staining the fixed cells with propidium iodide (PI).[47] We examined the effects of complexes **1** and **3**, which displayed the most prominent cytotoxicity, in comparison to CDDP as a reference compound; MDA-MB-231 cells were seeded at a density of 3×10^5 cells per well into 6-well plates (Thermo Scientific Nunc™) in the nutrition medium. After 24 h of growth, the cells were continually exposed to complexes **1** and **3** or CDDP at concentrations corresponding to $0.5 \times IC_{50}$ and IC_{50}: complex **1** (11 μM and 22 μM), complex **3** (13 μM and 26 μM) and CDDP (8 μM and 16 μM). After 24 h of treatment, cells were collected by trypsinization, washed twice with ice-cold PBS, and fixed for 30 min in 70% ethanol. Fixed cells were washed again with PBS and incubated with RNaseA (1 mg mL^{-1}) for 30 min at 37 °C. Immediately before flow-cytometric analysis, cells were stained with PI at a concentration of 400 μg mL^{-1}. The cell cycle phase distribution was analyzed using a fluorescence activated cell sorting (FACS) Calibur Becton Dickinson flow cytometer and Cell Quest computer software (Becton Dickinson, Heidelberg, Germany).

Annexin V-FITC apoptotic assay

Quantitative analysis of apoptotic and necrotic death of MDA-MB-231 cells induced by complexes **1** and **3** and CDDP as a reference compound were performed using an Annexin V-FITC apoptosis detection kit according to the manufacturer's instructions (BD Biosciences, Pharmingen San Diego, CA, USA). Briefly, 1×10^6 cells per mL were treated with complexes **1** and **3** and CDDP at concentrations corresponding to $0.5 \times IC_{50}$ and IC_{50} for 24 h. After treatment, the cells were collected, washed twice with ice-cold PBS and then resuspended in 200 μL 1× Binding Buffer (10 mM HEPES/NaOH pH 7.4, 140 mM NaCl, 2.5 mM $CaCl_2$). 100 μL of cell suspension (containing approximately 1×10^5 cells) was transferred to a 5 mL culture tube and mixed with 5 μL of both Annexin V-FITC and PI. The cells were gently vortexed and incubated for 15 min at 25 °C in the dark. After the incubation period, 400 μL of 1× Binding Buffer was added to each sample, which was then analyzed using a FACS Calibur Becton Dickinson flow cytometer and Cell Quest computer software (Becton Dickinson, Heidelberg, Germany).

Measurement of intracellular reactive oxygen species

Generation of reactive oxygen species (ROS) in MDA-MB-231 cells after treatment with complexes **1** and **3** and CDDP was measured using a ROS-sensitive fluorophore, 2′,7′-dichlorodihydrofluorescein diacetate (DCFH-DA, Sigma-Aldrich Co).[48] Briefly, 3×10^5 MDA-MB-231 cells per well were seeded into 6-well plates (Thermo Scientific Nunc™) in nutrition medium. After 24 h of growth, the cells were treated with complexes **1** and **3** and CDDP at concentrations corresponding to their IC_{50} values for 4 h. After treatment, the cells were harvested, washed twice with ice-cold PBS, re-suspended in 1 mL of 50 μM DCFH-DA and incubated for 30 min at 37 °C in the dark. After incubation with the dye, the cells were washed with PBS, re-suspended in 300 μL of PBS and immediately analyzed using the FL1 channel of the FACS Calibur Becton Dickinson flow cytometer and using Cell Quest computer software (Becton Dickinson, Heidelberg, Germany). The excitation wavelength used in the measurements was 485 nm, with peak emission measured at 530 nm. Subsequently, the geomean of the DCFH-DA-dependent fluorescence was determined.

Antioxidant activity

The antioxidant activities of complexes **1–4** were evaluated *via* their ability to scavenge free radicals such as DPPH, hydroxyl and ABTS. Furthermore, their ability to inhibit the activity of soybean lipoxygenase was also studied. Each experiment was performed in triplicate, and the standard deviation of absorbance was less than 10% of the mean.

Determination of the reducing activity of the stable radical DPPH. To an ethanolic solution of DPPH (0.1 mM), an equal volume of an ethanolic solution of the compound was added. The concentration of the solution of the compound was 0.1 mM. Ethanol was also used as a control solution. The absorbance at 517 nm was recorded at room temperature after 20 and 60 min in order to examine the time-dependence of the DPPH radical scavenging activity.[49a,b] The DPPH radical scavenging activity of the compounds was expressed as the percentage reduction of the absorbance value of the initial DPPH solution (RA%). NDGA and BHT were used as reference compounds.

Competition of the tested compounds with DMSO for hydroxyl radicals. The hydroxyl radicals generated by the Fe^{3+}/ascorbic acid system were detected by the determination of formaldehyde produced from the oxidation of DMSO, according to Nash.[50] The reaction mixture contained EDTA (0.1 mM), Fe^{3+} (167 μM), DMSO (33 mM) in phosphate buffer (50 mM, pH 7.4), the tested compound (concentration 0.1 mM) and ascorbic acid (10 mM). After 30 min of incubation (37 °C) the reaction was stopped with CCl_3COOH (17% w/v) and the absorbance at λ = 412 nm was measured. Trolox was used as an appropriate standard. The competition of the compounds with DMSO for $^{\bullet}OH$ generated by the Fe^{3+}/ascorbic acid system, expressed as the percent inhibition of formaldehyde production, was used for evaluation of their hydroxyl radical scavenging activities ($^{\bullet}OH$%).

Assay of radical cation scavenging activity. ABTS radical cation ($ABTS^{+\bullet}$) was produced by reacting an aqueous stock solution (2 mM) of ABTS with 0.17 mM potassium persulfate and allowing the mixture to stand in the dark at room temperature for 12 to 16 h before use. Because ABTS and potassium persulfate react stoichiometrically at a ratio of 1 : 0.5, this will result in incomplete oxidation of the ABTS. Although the oxidation of the ABTS commenced immediately, the absorbance became maximal and stable after 6 h. The radical was stable in this form for more than 2 days when stored in the dark

 This journal is © The Royal Society of Chemistry and the Centre National de la Recherche Scientifique 2018

Published on 11 January 2018. Downloaded by National Library of Serbia on 5/30/2020 12:11:45 PM.

at room temperature. The $ABTS^{+\bullet}$ solution was diluted with ethanol to an absorbance of 0.70 at 734 nm. After addition of 10 μL of diluted compound or standard (0.1 mM) in DMSO, the absorbance reading was taken exactly 1 min after the initial mixing.[49a] The radical scavenging activity of the complexes was expressed as the percentage inhibition of the absorbance of the initial ABTS solution (ABTS%). Trolox was used as an appropriate standard.

Soybean lipoxygenase inhibition study *in vitro*. The *in vitro* soybean lipoxygenase inhibition was evaluated as reported previously.[49a] The tested compounds were dissolved in ethanol and were incubated at room temperature with sodium linoleate (0.1 mM) and 0.2 mL of enzyme solution ($1/9 \times 10^{-4}$ w/v in saline). The conversion of sodium linoleate to 13-hydroperoxylinoleic acid at 234 nm was recorded and compared with the appropriate standard inhibitor caffeic acid.

Albumin binding studies

The albumin binding studies were performed by tryptophan fluorescence quenching experiments using bovine serum albumin (BSA, 3 μM) or human serum albumin (HSA, 3 μM) in buffer (containing 15 mM trisodium citrate and 150 mM NaCl at pH 7.0). The quenching of the emission intensity of tryptophan residues of BSA at 343 nm or HSA at 351 nm was monitored using complexes **1–4** as quenchers with increasing concentration.[51] The fluorescence emission spectra were recorded in the range of 300 to 500 nm with an excitation wavelength of 295 nm. The fluorescence emission spectra of the free compounds were also recorded under the same experimental conditions, *i.e.* excitation at 295 nm; the complexes bearing indomethacin ligands (*i.e.* **1** and **3**) exhibited a low emission band at ~365 nm,[22] while those bearing mefenamato ligands (*i.e.* **2** and **4**) did not exhibit any appreciable emission bands.[30] Therefore, in order to perform quantitative studies of the interaction with serum albumins, the fluorescence emission spectra of the indomethacin complexes **1** and **3** were corrected by subtracting the spectra of the compounds. The influence of the inner-filter effect[52] on the measurements was evaluated by eqn (S1) (ESI†). The Stern–Volmer and Scatchard equations (eqn (S2)–(S4), ESI†) and graphs[53a–c] were used in order to calculate the Stern–Volmer constant K_{SV} (in M^{-1}), the SA-quenching constant (k_q, in $M^{-1}\ s^{-1}$), the SA-binding constant K (in M^{-1}) and the number of binding sites per albumin (n).

DNA binding studies

The interaction of complexes **1–4** with CT DNA was studied by UV-vis spectroscopy in order to investigate the possible binding modes to CT DNA and to calculate the DNA-binding constants (K_b). The UV-vis spectra of CT DNA (0.15 to 0.18 mM) were recorded in the presence of each compound with diverse [complex]/[DNA] mixing ratios (= r). The K_b constants (in M^{-1}) were determined by the Wolfe–Shimmer equation (eqn (S5), ESI†)[54a,b] and the plots of $[DNA]/(\varepsilon_A - \varepsilon_f)$ *versus* [DNA] using the UV-vis spectra of the complex (50 to 100 μM) recorded in the presence of DNA for diverse r values.[55a] Control experiments with DMSO were performed, and no changes in the spectra of CT DNA were observed.

The viscosity of DNA ([DNA] = 0.1 mM) in buffer solution (150 mM NaCl and 15 mM trisodium citrate at pH 7.0) was measured in the presence of increasing amounts of complexes **1–4** (up to the value of r = 0.35). All measurements were performed at room temperature. The obtained data are presented as $(\eta/\eta_0)^{1/3}$ *versus* r, where η is the viscosity of DNA in the presence of the compound and η_0 is the viscosity of DNA alone in buffer solution.

The competitive studies of complexes **1–4** with EB were investigated by fluorescence emission spectroscopy in order to examine if the complexes could displace EB from its CT DNA–EB conjugate. The CT DNA–EB conjugate was prepared by adding 20 μM EB and 26 μM CT DNA in buffer (150 mM NaCl and 15 mM trisodium citrate at pH 7.0). The intercalating effects of the complexes were studied by stepwise addition of a certain amount of a solution of the compound into a solution of the DNA–EB conjugate. The influence of the addition of each compound to the DNA–EB complex solution was obtained by monitoring the changes of the fluorescence emission spectra recorded with an excitation wavelength (λ_{ex}) at 540 nm. Complexes **1–4** did not show any fluorescence emission bands at room temperature in solution or in the presence of CT DNA or EB under the same experimental conditions (λ_{ex} = 540 nm); therefore, the observed quenching is attributed to the displacement of EB from its EB–DNA conjugate. The Stern–Volmer constants (K_{SV}, in M^{-1}) were calculated according to the linear Stern–Volmer equation (eqn (S2), ESI†)[53b] and the plots of I_0/I *versus* [Q]. The quenching constants (k_q, in $M^{-1}\ s^{-1}$) of the complexes were calculated according to eqn (S3) (ESI†) because the fluorescence lifetime of the EB–DNA system is τ_0 = 23 ns.[55b]

Results and discussion

Synthesis and characterization of Ru complexes

Reaction of $[Ru(\eta^6\text{-arene})Cl_2]_2$, namely $[Ru(\eta^6\text{-}p\text{-cymene})Cl_2]_2$ or $[Ru(\eta^6\text{-toluene})Cl_2]_2$, with stoichiometric amounts of the corresponding NSAID ligands, indomethacin (Hindo) and mefenamic acid (Hmef), led to the formation of two cymene complexes, $[Ru(\eta^6\text{-}p\text{-cymene})(indo)Cl_2]^-$ **1** and $[Ru(\eta^6\text{-}p\text{-cymene})(mef)Cl_2]^-$ **2**, and two toluene complexes, $[Ru(\eta^6\text{-toluene})(indo)Cl_2]^-$ **3** and $[Ru(\eta^6\text{-toluene})(mef)Cl_2]^-$ **4**, in reasonably good yields. The resulting complexes **1** and **3** precipitated after neutralization with potassium hydroxide, and complexes **2** and **4** precipitated after addition of ammonium hexafluorophosphate to the reaction mixture (Scheme 1). Complexes **1** and **3** showed good solubility in acetonitrile, dimethylsulfoxide, and chloroform and lower solubility in ethanol and methanol. Complexes **2** and **4** showed excellent solubility in all these solvents.

The IR spectra of the free NSAIDs show characteristic absorption bands for the ν(O–H) vibration at about 3500 cm^{-1}. These absorption bands did not appear in the IR spectra of the complexes, indicating ligand coordination *via* carboxylate anions. Due to this, the coordination absorption bands for carbonyl group stretching at 1650 to 1700 cm^{-1} in the complexes were also slightly shifted to lower values.

Published on 11 January 2018. Downloaded by National Library of Serbia on 5/30/2020 12:11:45 PM.

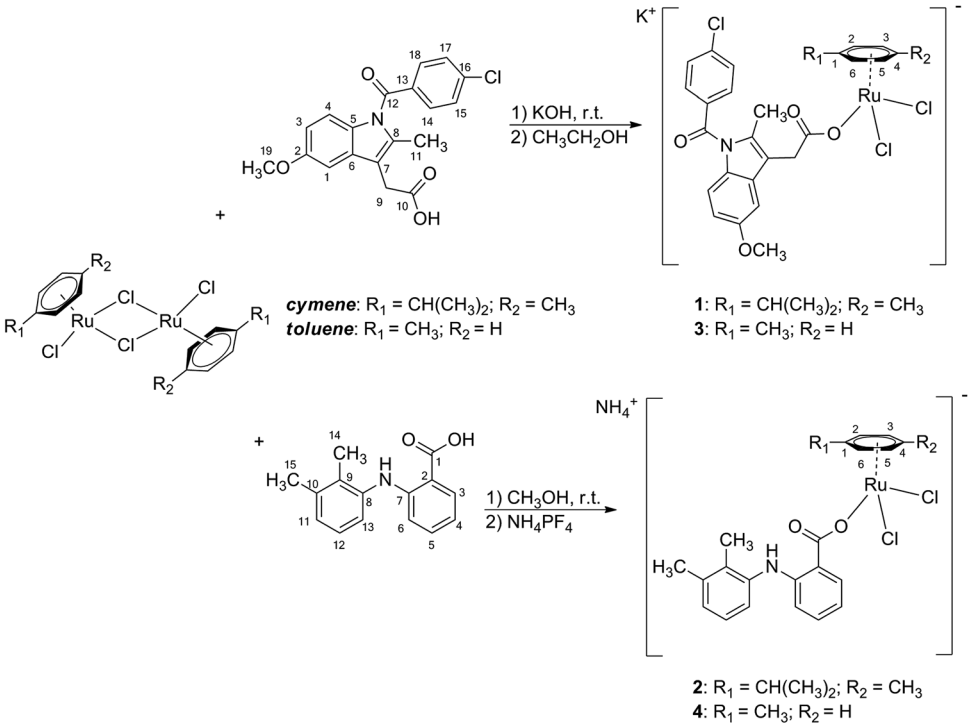

Scheme 1 Reaction scheme for the synthesis of complexes **1–4**.

Upon complexation to the metal, the symmetries of [Ru(η^6-*p*-cymene)Cl$_2$]$_2$ and [Ru(η^6-toluene)Cl$_2$]$_2$ decreased. The cymene and toluene ring protons as well as the protons from the ligand moiety in the complexes exhibited slightly lower chemical shifts in comparison to the starting complexes or the ligands themselves. Signals for protons from the carboxylic group in the ^{1}H NMR spectra of all complexes did not appear due to deprotonation and coordination.

The ^{13}C NMR spectra of the synthesized complexes did not suffer significant changes. Chemical shifts for carbon atoms from the arene moiety were slightly moved to higher values. Values for chemical shifts corresponding to carbon atoms from the carboxylate groups were higher in the complexes compared to the free ligands (Fig. S1–S8, ESI†).

Finally, mass spectra of the complexes were recorded both in positive and negative ion mode. The molecular ion was detected only in the case of complex **3**, *m*/*z* values 621.9 in negative mode and 623 in positive mode, while in other cases, only the anionic parts of the complexes with or without Cl ions were detected: $[M - K^+ - 2Cl + H]^+$ (**1**, **3**) and $[M - NH_4 - 2Cl]^+$ (**2**, **4**).

MTT assay

The cytotoxic activities of the novel ruthenium(II) complexes **1–4**, as well as the free NSAID ligands, indomethacin and mefenamic acid, in comparison to cisplatin (CDDP) were investigated by MTT assay. The study was performed in three human cancer cell lines (K562, A549, MDA-MB-231) and in one human non-tumor cell line (MRC-5). The results obtained after 72 h of continuous drug action are presented as IC_{50} values (μM) (Table 1) provided from cell survival diagrams (Fig. 2). Complexes **1–4** exhibited generally higher cytotoxic activity compared to free NSAIDs, Hindo and Hmef, although the IC_{50} values of complexes varied in the micromolar range from 11.9 to 275.7 μM depending on the cell line. Complexes **1** and **3**, carrying indomethacin ligands, showed the highest cytotoxic potential. The human myelogenous leukemia K562 cell line proved to be the most sensitive to the actions of **1** and **3** (IC_{50} values: 11.9 μM and 13.2 μM, respectively). These values were comparable to cisplatin (IC_{50} = 10.3 μM), and were significantly lower than the IC_{50} values obtained for complexes **2** (IC_{50} = 96.4 μM), and **4** (IC_{50} = 133 μM). Interestingly, MDA-MB-231 cells exhibited much greater sensitivity toward **1** and **3** than CDDP-resistant lung carcinoma A549 cells and non-tumor MRC-5 cells. The results for MRC-5 indicated that this cell line was at least 4 times less sensitive to **1–4** than to CDDP. The NSAIDs exhibited poor activity, up to 300 μM, while Hmef could be considered inactive in MRC-5. A structure–activity comparison revealed that

Table 1 IC_{50} values (μM) obtained after 72 h of continuous drug action[a]

Compound	K562	A549	MDA-MB-231	MRC-5
1	11.9 ± 4.4	45.5 ± 2.7	22 ± 3.6	39.6 ± 3.7
2	96.4 ± 2	145.1 ± 6.4	153 ± 1.2	222.6 ± 23.9
3	13.2 ± 6.2	31.7 ± 1.15	26 ± 1.7	42 ± 1.3
4	133 ± 7	142.4 ± 9.3	121.4 ± 1.8	275.7 ± 14.5
Hindo	155.9 ± 11.4	161.5 ± 13.9	244.7 ± 17.8	230.5 ± 17.8
Hmef	143.9 ± 4.1	217.3 ± 46.7	237.9 ± 18.8	>300
CDDP	10.3 ± 1.2	13.6 ± 1.8	15.9 ± 2.1	9.3 ± 0.9

[a] IC_{50} values (μM) are presented as the mean ± SEM of three independent experiments. >300 denotes that IC_{50} was not obtained in the range of concentrations tested up to 300 μM.

 This journal is © The Royal Society of Chemistry and the Centre National de la Recherche Scientifique 2018

Published on 11 January 2018. Downloaded by National Library of Serbia on 5/30/2020 12:11:45 PM.

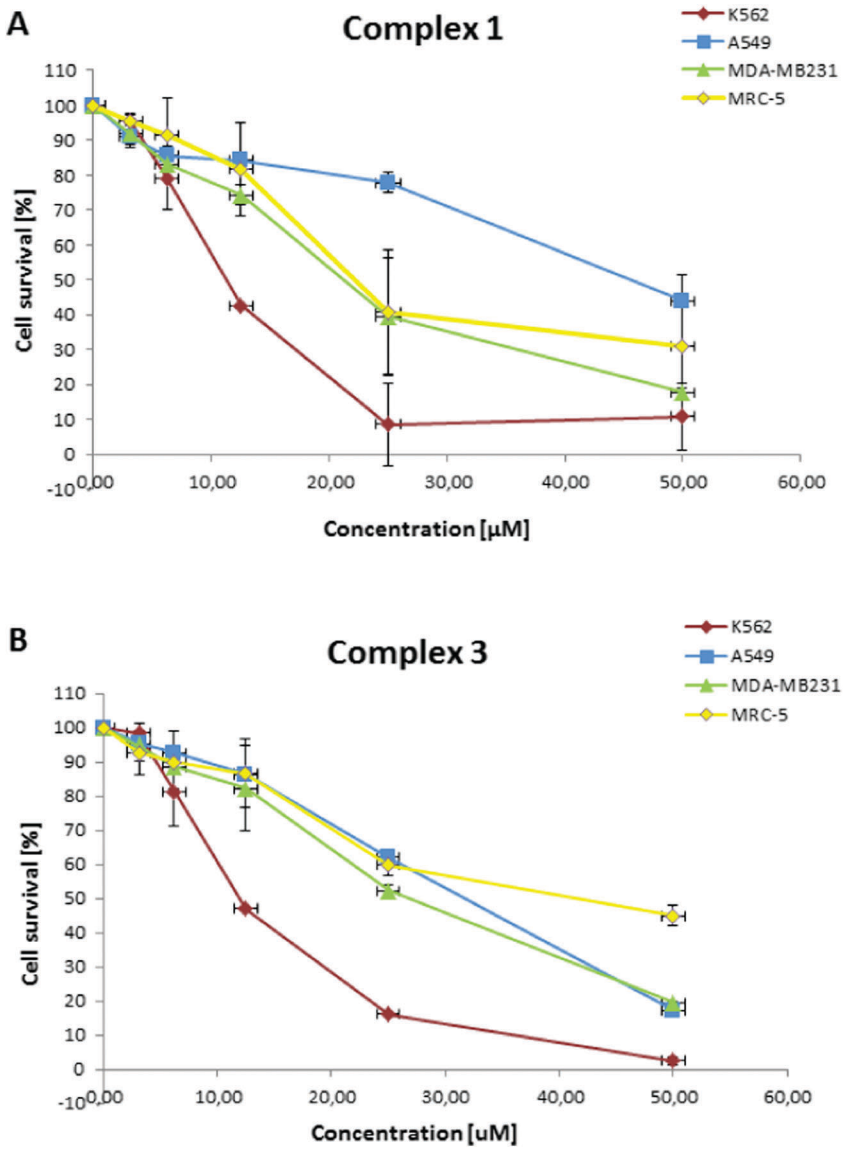

Fig. 2 Cell survival curves after 72 h of treatment of K562, A549, MDA-MB-231 and MRC-5 cell lines with (A) complex **1** and (B) complex **3**.

the NSAID Hindo enhanced the cytotoxicity of the resulting ruthenium(II)–arene complexes **1** and **3** despite having poor activity itself. On the other hand, π-bonded arene ligands such as *p*-cymene (in complexes **1** and **2**) or toluene (in complexes **3** and **4**) appeared to have no significant impact on the *in vitro* cytotoxic potential of the complexes. Triple-negative breast cancer cells such as MDA-MB-231 are characterized by high metastatic potential and lack of specific molecular targets for effective therapy; thus, the results of the present study indicated that ruthenium-based "combi-molecules" may represent a promising alternative for treatment of this type of cancer (Table S1, ESI†).

Cell cycle analysis

The capability of complexes **1**, **3** and CDDP to induce cell cycle alterations was examined by flow cytometry after 24 h of continual treatment and staining with PI. Triple-negative breast carcinoma MDA-MB-231 cells were chosen to further investigate the mechanism of action of complexes **1** and **3**. The results are presented in Fig. 3 as diagrams of cell distribution over the cell cycle phases. At low 0.5 × IC_{50} concentrations, both **1** and **3** affected cell cycle progression in a manner different from that of cisplatin, causing slight accumulation of cells in G2-M phase and a decrease in G1 phase. Cell cycle changes progressed at higher concentrations of the tested complexes **1** and **3** (IC_{50}) and were characterized by rapid accumulation of cells in sub-G1, up to 48.5% (**1**) and 47.09% (**3**) compared to the control (0.03%). There was a decrease in the cell population in the G2-M and G1 phases and arrest in the S phase of the cell cycle, up to 18.66% (**1**) and 20.95% (**3**) *versus* the control (14.24%). Obviously, cells that could not progress through S phase following action of **1** and **3** (at IC_{50}) entered cell death and accumulated in sub-G1 phase. Formation of the Sub-G1 or hypodiploid peak is considered to be a hallmark of fragmented DNA.[56,57] Further UV-vis spectroscopic studies also

Published on 11 January 2018. Downloaded by National Library of Serbia on 5/30/2020 12:11:45 PM.

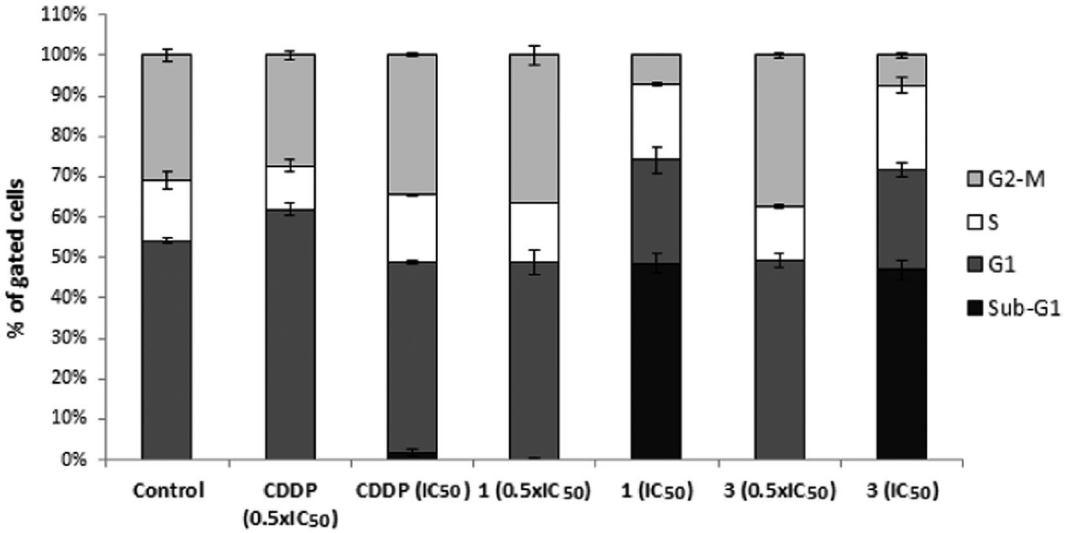

Fig. 3 Diagrams of cell cycle phase distributions of treated MDA-MB-231 cells after 24 h of treatment with complexes **1**, **3** and CDDP at concentrations corresponding to 0.5 × IC_{50} and IC_{50}.

demonstrated the potential of complexes **1** and **3** to bind to DNA (Table 4) and support these findings. The potential of different metal ions conjugated to NSAIDs to damage DNA and alter the cell cycle was previously demonstrated.[58–60] Recent investigation by Kasparkova and colleagues[58] of new Pt(II) conjugates carrying the NSAID diclofenac demonstrated their potential to act as a so-called ''combi-molecule'' which combines the DNA-binding properties of the metal center and antitumor properties of NSAID ligands for cytotoxic activity. The results of the present study strongly suggested the ability of complexes **1** and **3** to cause damage to DNA and arrest DNA replication, either through direct DNA-binding or by an indirect mechanism.

Annexin V-FITC apoptotic assay

Because MDA-MB-231 cells exhibited particular sensitivity to the cytotoxic action of complexes **1** and **3** (IC_{50} value), showing an intense Sub-G1 peak, we further investigated whether the apoptotic or necrotic changes underlie the mechanism of cell death. The potential of the investigated compounds or CDDP to induce apoptosis/necrosis in MDA-MB-231 cells was assessed by flow cytometry following Annexin-V-FITC/PI dual staining after 24 h of continual drug treatment. The results (Fig. 4A) show the percentage of early apoptotic cells, labeled FITC(+)/PI(−), late apoptotic cells, FITC(+)/PI(+), and necrotic cells, FITC(−)/PI(+).

The obtained experimental data indicated that both complexes **1** and **3** as well as CDDP initiated apoptosis in a concentration-dependent manner. At 0.5 × IC_{50} concentrations, **1** and **3** caused 7.96% and 6.73% of FITC(+)/PI(−) staining, respectively. These values were comparable to those of cisplatin, where 6.75% of cells were apoptotic, *versus* 4.41% in the control. As the dose of the compounds increased, the cells shifted from the healthy state, FITC(−)/PI(−), to either early apoptotic, FITC(+)/PI(−), or necrotic, FITC(+)/PI(+). Particularly significant dose-dependent effects on the cell redistribution between quadrants were observed after treatment with complexes **1** and **3**. At IC_{50} concentrations of **1** and **3**, percentages of early apoptotic cells increased up to 20%, which is 3 times more than for the cells treated with CDDP. Simultaneously, FITC(+)/PI(+) staining, characteristic for necrosis, increased up to 20%. Results of the Annexin-V-FITC/PI apoptosis assay are in accordance with the cell cycle study, which confirmed that under the same treatment conditions (IC_{50}, 24 h), more than 40% of cells underwent DNA-fragmentation and accumulated in Sub-G1 phase as either apoptotic or necrotic cells.

Measurement of intracellular reactive oxygen species

To investigate whether induced cytotoxic and apoptotic effects of synthesized ruthenium(II)–arene complexes **1** and **3** are related to ROS production, we measured the intracellular ROS levels in MDA-MB-231 cells after 4 h of treatment with the tested complexes **1** and **3** or CDDP at concentrations corresponding to their IC_{50} values. As illustrated in Fig. 5A, the ROS level did not change significantly after 4 h exposure to CDDP. However, after 4 h of treatment with complexes **1** and **3**, slight changes in the shapes of the fluorescent signal curves can be noted. Fluorescence of DCFH-DA in the treated cells is red-shifted toward a higher intensity compared to the control cells (Fig. 5B). This shift implies modest production of intracellular reactive oxygen species for 3.9% of cells treated with **1** and 5.42% of cells treated with **3**; these values are higher than those of the control cells (2%) and cisplatin (1.88%) (Fig. 5C). However, a study of the scavenging abilities of the tested complexes for DPPH, superoxide radical and hydroxyl radical showed that complex **1** exhibited the highest ROS scavenging properties. Certainly, additional studies are needed in order to precisely address the features of the tested complexes that dominate the mechanisms of their cytotoxic action. The noticeable changes in ROS levels under treatment at an early time point (4 h) suggest that these complexes exhibit a strong,

 This journal is © The Royal Society of Chemistry and the Centre National de la Recherche Scientifique 2018

Published on 11 January 2018. Downloaded by National Library of Serbia on 5/30/2020 12:11:45 PM.

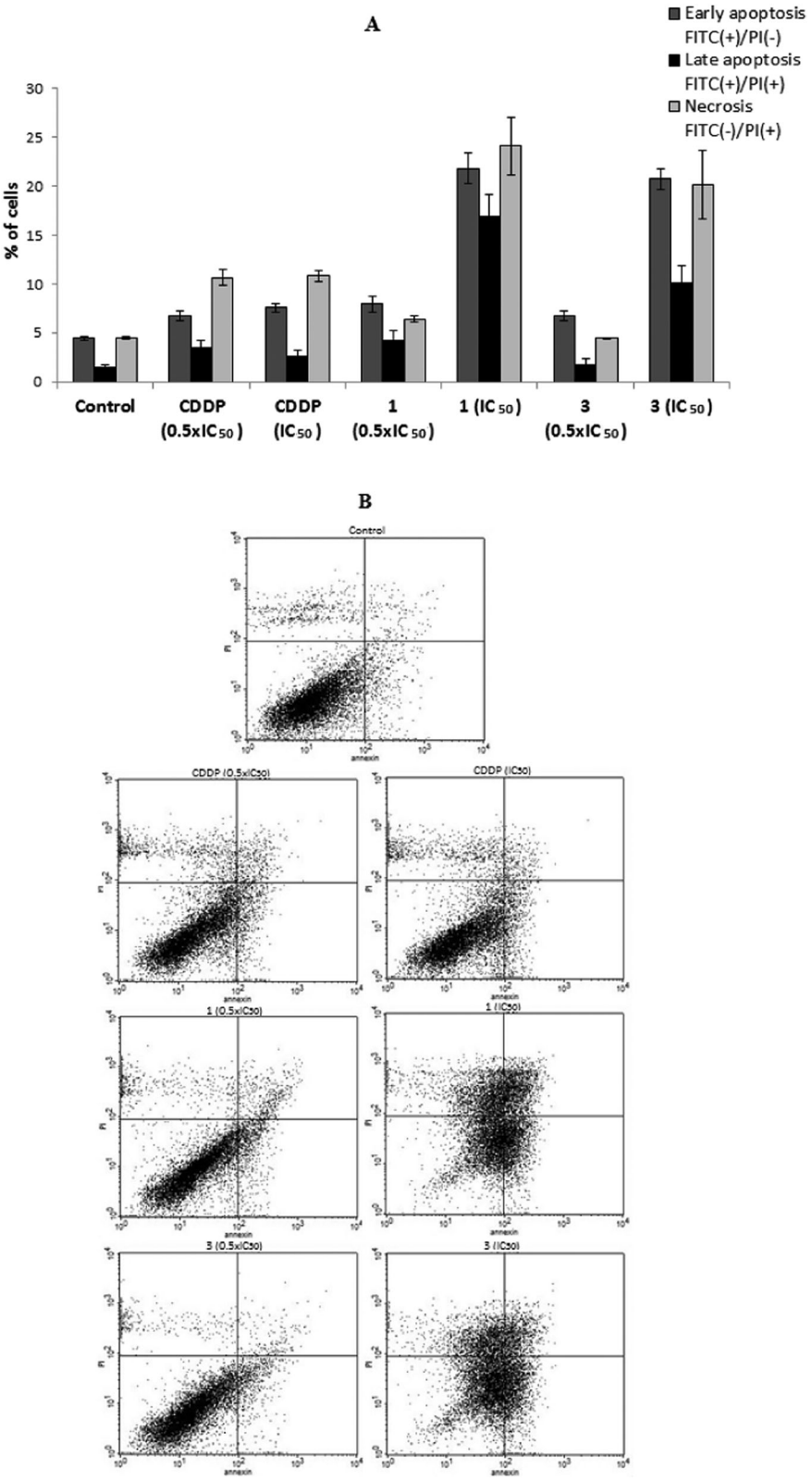

Fig. 4 (A) Bar graph of apoptosis and necrosis, quantified by FACS, after Annexin V-FITC and PI labelling. (B) Dot plot diagrams following 24 h treatment of MDA-MB-231 cells with complexes **1** and **3** or CDDP at concentrations corresponding to 0.5 × IC_{50} and IC_{50}. Representative dot plots of three independent experiments are given, presenting intact cells in the lower-left quadrant, FITC(−)/PI(−); early apoptotic cells in the lower-right quadrant, FITC(+)/PI(−); late apoptotic or necrotic cells in the upper-right quadrant, FITC(+)/PI(+); and necrotic cells in the upper-left quadrant, FITC(−)/PI(+).

Published on 11 January 2018. Downloaded by National Library of Serbia on 5/30/2020 12:11:45 PM.

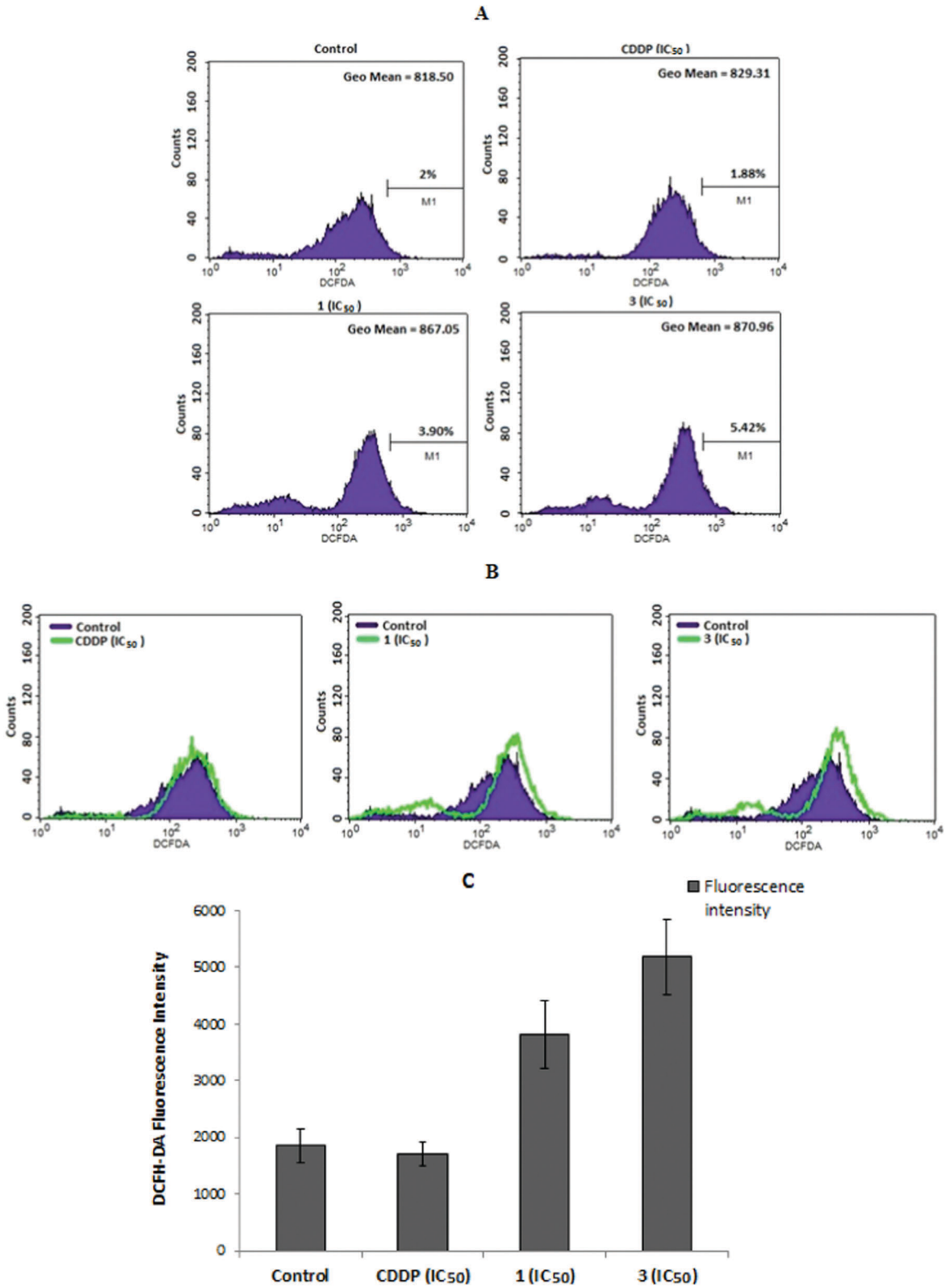

Fig. 5 Effects of complexes **1**, **3** and CDDP on intracellular ROS levels. MDA-MB-231 cells were treated for 4 h with the tested compounds at concentrations corresponding to their IC_{50} values and subjected to flow cytometry-based oxidative stress analysis for measurement of the ROS levels. Intracellular oxidative stress is indicated on the horizontal axis and corresponds to the fluorescence intensity of DCFH-DA. The vertical axis shows the cell numbers. (A) Representative histograms of one of three independent experiments, presenting the percentage of increase of ROS accumulation in treated cells relative to control cells; (B) enhancement of intracellular ROS accumulation, observed *via* the shift of the signal curve obtained for the treated cells (presented as a line) to the right compared with that of the control cells (presented as a filled curve); (C) bar graph presenting the mean fluorescence intensities of DCFH-DA of three independent experiments.

 This journal is © The Royal Society of Chemistry and the Centre National de la Recherche Scientifique 2018

Published on 11 January 2018. Downloaded by National Library of Serbia on 5/30/2020 12:11:45 PM.

multiple-layer cytotoxic effect, possibly triggered by ROS release and afterwards by induction of cell death. Previous literature data on the *in vitro* antitumor effects of NSAID agents, such as acetylsalicylic acid (aspirin), reported their potential to synergistically enhance the cytotoxicity of cisplatin or other chemotherapeutic anticancer agents by different mechanisms, including cell cycle alteration or induction of apoptosis through oxidative stress and mitochondrial dysfunction.[59,61–63] The results of the present study signify that NSAIDs conjugated with ruthenium–arenes represent a promising class of agents with unique *in vitro* anti-tumor features resulting from the combined properties of both ruthenium–arenes and NSAIDs.

Antioxidant activities of the complexes

Compounds that can scavenge free radicals or inhibit their production have potential applications in the treatment of inflammation[49a,b] because free radicals are species involved in the inflammatory process. Within this context, the *in vitro* antioxidant activities of complexes **1–4**, *i.e.* the *in vitro* scavenging activities of complexes **1–4** towards DPPH, ABTS and hydroxyl radicals, and their ability to inhibit the activity of soybean lipoxygenase have been studied and have been compared to the well-known antioxidant agents NDGA, BHT, trolox and caffeic acid, which were used as standard reference compounds (Table 2).

The ability of complexes **1–4** to scavenge DPPH radicals (which is usually closely related to antiageing, anticancer and anti-inflammatory activity)[49a,b] was time-independent because no significant differences were observed after treatment for 20 min and 60 min. On average, complexes **1–4** were better DPPH-scavengers than the corresponding free NSAIDs Hindo and Hmef but less active than the reference compounds BHT and NDGA. Complexes **1** and **3**, bearing indomethacin ligands, were more potent than their analogues **2** and **4**, respectively. Complex **1** was found to be the best DPPH-scavenger among the present complexes.

The scavenging of hydroxyl radicals ($^{\bullet}$OH) usually indicates that the compounds may offer relief from the presence of reactive oxygen species.[49a,b] The scavenging ability of the complexes towards hydroxyl radicals is significantly high; all complexes **1–4** were more active than the corresponding free NSAIDs, Hindo and Hmef, and more active than the reference compound trolox. Complexes **1** and **2**, which contain the arene *p*-cymene, are the most active hydroxyl-scavengers among the present compounds.

The scavenging of cationic ABTS radicals ($ABTS^{+\bullet}$) is often used as a marker of total antioxidant activity.[49a] Regarding the ABTS scavenging ability of complexes **1–4**, the complexes are more active than the corresponding free NSAIDs, Hindo and Hmef, but less active than the reference compound trolox. Complexes **1** and **3** bearing indomethacin as a ligand are better ABTS-scavengers than their mefenamato analogues **2** and **4**, respectively. Complex **1** is the most active ABTS-scavenger among complexes **1–4**.

Compounds that can inhibit the activity of LOX may be considered as potential antioxidants or free radical scavengers because lipoxygenation is a procedure which usually occurs *via* a carbon-centered radical.[64] In comparison with the reference compound caffeic acid, complexes **1–4** are very potent LOX inhibitors, with the indomethacin complexes **1** and **3** being the most active compounds.

In general, complexes **1–4** are better radical scavengers than the corresponding free NSAIDs Hindo and Hmef, suggesting that their coordination to Ru(II) results in enhanced scavenging activity. In comparison with reported metal–NSAID analogues,[17,22,29–33,65–69] the present complexes **1–4** are significantly active DPPH-, ABTS- and hydroxyl-scavengers and LOX-inhibitors. Although the number of the present compounds is rather low to clarify the structural factors that lead to enhanced antioxidant activity, we suggest that the complexes bearing indomethacin and/or *p*-cymene are the most potent compounds; as a result, complex **1** was found to be the most active compound. Furthermore, the complexes are more active scavengers of hydroxyl and ABTS radicals than of DPPH radicals; this scavenging selectivity for hydroxyl and ABTS radicals has been previously reported in the literature,[70–72] especially for metal–NSAID complexes.[17,22,29–33,65–69]

Interaction with biomolecules

Interaction of the complexes with albumins. The most important role of the serum albumins (SAs) is the transportation of ions and drugs towards their biological targets, *i.e.* cells and tissues.[50] Within this context, the study of the interaction of biologically potent compounds (such as the reported complexes **1–4**) with SAs can be considered as an approach for the exploration of potential biological activity and applications. As a result of this interaction, the biological properties of

Table 2 %DPPH scavenging ability (RA%), % superoxide radical scavenging activity (ABTS%), competition with DMSO for hydroxyl radical ($^{\bullet}$OH%), and *in vitro* inhibition of soybean lipoxygenase (LOX, IC_{50} in μM) for Hindo and Hmef and their complexes **1–4**

Compound	RA%, 20 min	RA%, 60 min	$^{\bullet}$OH%	ABTS%	LOX
1	34.23 ± 0.35	33.26 ± 0.66	96.89 ± 0.33	88.11 ± 0.92	29.76 ± 0.12
2	13.67 ± 0.35	15.16 ± 0.42	96.58 ± 0.11	78.21 ± 0.27	34.56 ± 0.17
3	26.58 ± 0.41	25.42 ± 0.17	93.41 ± 0.16	82.54 ± 0.23	27.34 ± 0.55
4	8.82 ± 0.47	9.24 ± 0.48	93.56 ± 0.38	72.61 ± 0.86	40.54 ± 0.73
Hindo	20.32 ± 0.73	24.65 ± 0.47	91.34 ± 0.74	79.64 ± 0.30	34.46 ± 0.59
Hmef	5.72 ± 0.08	11.74 ± 0.20	92.51 ± 0.44	66.32 ± 0.38	48.52 ± 0.88
NDGA	81.02 ± 0.18	82.60 ± 0.17	Not tested	Not tested	Not tested
BHT	31.30 ± 0.10	60.00 ± 0.38	Not tested	Not tested	Not tested
Trolox	Not tested	Not tested	82.80 ± 0.13	91.8 ± 0.17	Not tested
Caffeic acid	Not tested	Not tested	Not tested	Not tested	600 ± 0.3

Published on 11 January 2018. Downloaded by National Library of Serbia on 5/30/2020 12:11:45 PM.

the compounds may alter when bound to albumins, or novel alternative pathways or mechanisms of activity and transportation may be revealed.[73] Therefore, the interaction of complexes **1–4** with HSA and its homologue BSA were studied by fluorescence emission spectroscopy. The solutions of HSA and BSA exhibit intense fluorescence emission bands at $\lambda_{em,max}$ = 352 nm and 343 nm, respectively, with an excitation wavelength at 295 nm; this band is due to the presence of tryptophans, *i.e.* the tryptophan at position 214 in HSA and the tryptophans at positions 134 and 212 in BSA.[50]

The quenching in the fluorescence emission spectra of the SAs induced by the presence of the complexes was low for the complexes in the case of HSA (the quenching of the initial HSA fluorescence emission ($\Delta I/I_0$) reached ~49.3% in the presence of complex **3**, Fig. 6A) and was much more pronounced for BSA (the quenching of the initial BSA fluorescence emission ($\Delta I/I_0$) reached 74.8% in the presence of complex **2**, Fig. 6B). This quenching of the SA fluorescence emission band may be ascribed to possible changes in the tryptophan environment of SA and, subsequently, changes in the secondary structure of albumin arising from the binding of each complex to SA.[53a]

The quenching constants (k_q) of the interactions of the complexes with the albumins were calculated (Table 3) from the corresponding Stern–Volmer plots (Fig. S9 and S10, ESI†) and Stern–Volmer quenching equation (eqn (S2) and (S3), ESI†), where the fluorescence lifetime of tryptophan in SA was taken as $\tau_0 = 10^{-8}$ s;[52] the quenching constants are significantly higher than the value of 10^{10} M^{-1} s^{-1}, suggesting that the interaction of the complexes with the albumins takes place *via* a static quenching mechanism,[52] which indicates the formation of a new conjugate between each complex and the albumin. The k_q constants of complexes **1–4** may show significant SA-quenching ability for the complexes; this effect was more intense in the case of BSA, with complex **1** showing the highest k_q for HSA and complex **2** for BSA. The derived k_q constants for complexes **1–4** are within the range found for a series of metal-complexes bearing NSAIDs as ligands.[17,22,29–33,65–69]

The SA-binding constants (K) of the complexes have been determined (Table 3) from the corresponding Scatchard plots (Fig. S11 and S12, ESI†) and the Scatchard equation (eqn (S4), ESI†). The K constants of complexes **1–4** are all relatively high, similar to their respective free NSAIDs, and are in the range of the values calculated for metal–NSAID complexes.[17,22,29–33,65–69] Among the present complexes, complexes **4** and **1** bear the highest K constants for HSA and BSA, respectively. Considering the structural factors present in complexes **1–4**, it seems that complexes **1** and **2** bearing η^6-*p*-cymene ligands show higher binding activity for BSA than their analogues **3** and **4** bearing η^6-toluene ligands. In the case of HSA, we cannot confidently suggest a structural factor that leads to higher binding affinity.

The SA-binding constants of complexes **1–4** lie in the range of 4.24×10^4 to 4.49×10^5 M^{-1} (Table 3) and are high enough to reveal the potential binding of the complexes to SAs in order to enable transfer towards potential biotargets. Additionally, the K constants are significantly lower than the value of 10^{15} M^{-1}, *i.e.* the binding constant of avidin with diverse compounds,[74]

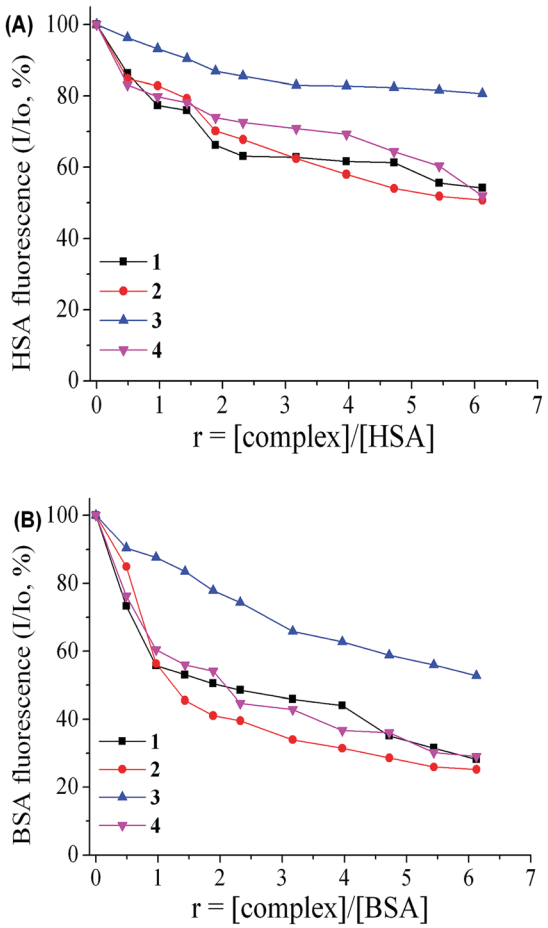

Fig. 6 (A) Plot of relative HSA fluorescence intensity at λ_{em} = 352 nm (I/I_0, %) *vs.* *r* (*r* = [complex]/[HSA]) for complexes **1–4** (up to 54.1% of the initial HSA fluorescence for **1**, 50.7% for **2**, 80.7% for **3** and 52.0% for **4**) in buffer solution (150 mM NaCl and 15 mM trisodium citrate at pH 7.0). (B) Plot of relative BSA fluorescence intensity at λ_{em} = 343 nm (I/I_0, %) *vs.* *r* (*r* = [complex]/[BSA]) for complexes **1–4** (up to 28.2% of the initial BSA fluorescence for **1**, 25.2% for **2**, 52.8% for **3** and 29.0% for **4**) in buffer solution (150 mM NaCl and 15 mM trisodium citrate at pH 7.0).

which is the strongest known non-covalent reversible interaction;[53c] this comparison may indicate reversible binding of the complexes to the SAs and may reveal the potential for release upon arrival at the desired target.

Interaction of the complexes with CT DNA. Covalent binding or noncovalent interactions are the most common interactions between metal complexes and double-stranded DNA. Covalent binding takes place when nitrogen atoms of DNA-bases displace one or more labile ligands of the complex, while the noncovalent interactions are: (i) intercalation, *i.e.* $\pi \rightarrow \pi$ stacking interactions between the complex and DNA nucleobases, (ii) electrostatic interactions, namely Coulomb forces developed between the complexes and the phosphate groups of DNA, and (iii) groove-binding, attributed to van der Waals or hydrogen-bonding or hydrophobic bonding interactions along the grooves of the DNA helix.[75a] The potential anticancer and/or anti-inflammatory activities of NSAIDs and their complexes are often related to their DNA-binding behavior.[17,75b] Within this context,

 This journal is © The Royal Society of Chemistry and the Centre National de la Recherche Scientifique 2018

Published on 11 January 2018. Downloaded by National Library of Serbia on 5/30/2020 12:11:45 PM.

Table 3 The albumin quenching and binding constants for complexes **1–4**

Compound	$k_{q(HSA)}$ (M^{-1} s^{-1})	$K_{(HSA)}$ (M^{-1})	$k_{q(BSA)}$ (M^{-1} s^{-1})	$K_{(BSA)}$ (M^{-1})
Hindo[22]	$7.80(\pm0.60) \times 10^{12}$	$2.22(\pm0.19) \times 10^{5}$	$7.68(\pm0.28) \times 10^{12}$	$8.95(\pm0.40) \times 10^{5}$
Hmef[30]	$7.13(\pm0.34) \times 10^{12}$	$1.32(\pm0.15) \times 10^{5}$	$2.78(\pm0.20) \times 10^{13}$	$1.35(\pm0.22) \times 10^{5}$
1	$6.10(\pm0.29) \times 10^{12}$	$2.15(\pm0.08) \times 10^{5}$	$1.25(\pm0.05) \times 10^{13}$	$4.49(\pm0.30) \times 10^{5}$
2	$5.46(\pm0.19) \times 10^{12}$	$9.79(\pm0.34) \times 10^{4}$	$1.70(\pm0.08) \times 10^{13}$	$3.63(\pm0.15) \times 10^{5}$
3	$2.04(\pm0.13) \times 10^{12}$	$9.44(\pm0.40) \times 10^{4}$	$4.85(\pm0.11) \times 10^{12}$	$5.30(\pm0.18) \times 10^{4}$
4	$4.32(\pm0.29) \times 10^{12}$	$4.24(\pm0.12) \times 10^{5}$	$1.30(\pm0.04) \times 10^{13}$	$2.63(\pm0.10) \times 10^{5}$

the DNA-binding affinities of complexes **1–4** were studied *in vitro* by UV-vis spectroscopy, viscosity measurements and their ability to displace the typical DNA-intercalator EB.

UV-vis spectroscopy is used as a preliminary method to examine the DNA-binding mode and to calculate its strength. Any changes observed in the DNA-band or the intraligand transition bands of the complexes may reveal the existence of interactions and their possible modes. The UV-vis spectra of a CT DNA solution in the presence of complex **4** at increasing *r* values are shown representatively in Fig. 7A. The band at λ_{max} = 258 nm exhibits a slight hypochromism accompanied by a red-shift up to 260 nm, suggesting the existence of interactions between CT DNA and the complex leading to the formation of a new complex-DNA conjugate[76] and resulting in stabilization of the CT DNA double-helix.[77] The behaviour of CT DNA in the presence of the other complexes is quite similar.

In the UV-vis spectra of complex **1** (Fig. 7B), the intraligand band observed at 321 nm exhibited in the presence of CT DNA showed slight hypochromism of up to 7%. Similar changes were observed in the UV-vis spectra of complex **3** in the presence of DNA (Table 4). In the UV-vis spectra of complex **4** (Fig. 7C), upon addition of CT DNA, the intraligand band located at 282 nm (I) presented a significant hyperchromism up to 20% followed by a significant red-shift of 15 nm; upon addition of CT DNA, the second band located at 349 nm (II) presented an intense hypochromism up to 50% followed by elimination. Similar spectroscopic features were observed in the UV-vis spectra of complex **2** in the presence of DNA (Table 4). Safe conclusions cannot be merely derived from UV-vis spectroscopic titration studies. Of course, the significant percentage of hypochromism observed for the mefenamato complexes **2** and **4** can be attributed to π→π stacking interactions between the aromatic chromophores of the complexes and DNA-bases[53b,c] and may be consistent with an intercalative binding mode, leading to stabilization of the DNA helix.[77] However, in order to clarify the DNA-binding modes of complexes **1–4**, DNA-viscosity measurements were performed.

The DNA-binding constants (K_b) of complexes **1–4** (Table 4) were calculated using the Wolfe–Shimer equation[53a] (eqn (S5), ESI†) and the corresponding plots of [DNA]/($\varepsilon_A - \varepsilon_f$) *versus* [DNA] (Fig. S13, ESI†). The K_b constants of complexes **1–4** (Table 4) are relatively high and suggest strong binding of the complexes to CT DNA. Considering the structural factors present in complexes **1–4**, it seems that the complexes bearing η^6-*p*-cymene ligands (**1** and **2**) show higher DNA-affinity than their analogues bearing η^6-toluene ligands (**3** and **4**); also, the complexes bearing mefenamato ligands (**2** and **4**) are better

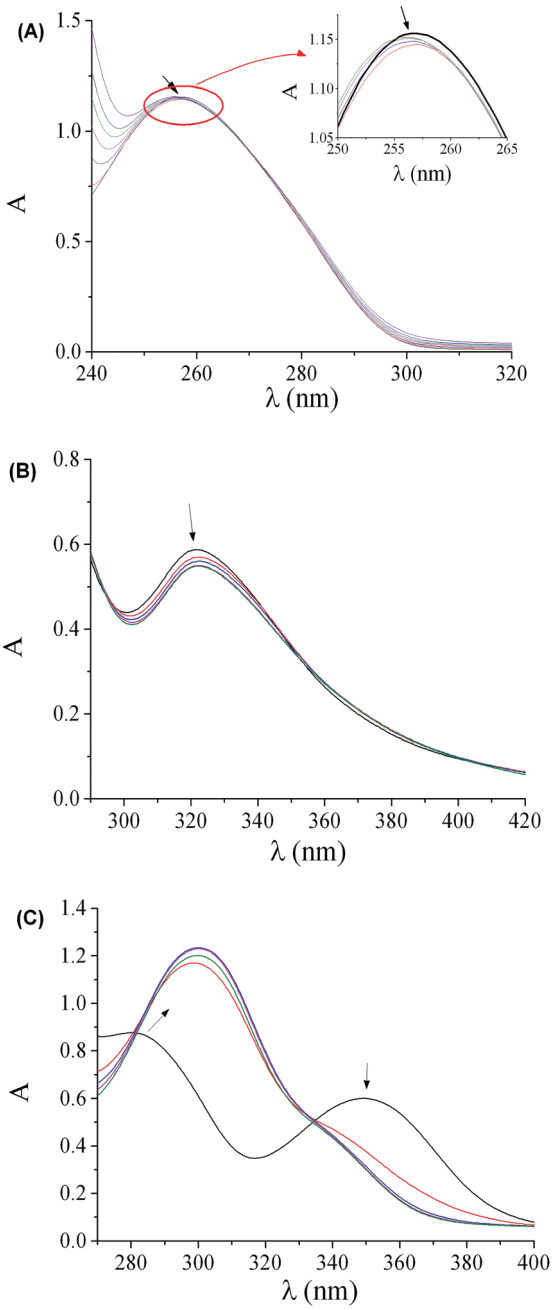

Fig. 7 (A) UV-vis spectra of CT DNA (0.175 mM) in buffer solution (150 mM NaCl and 15 mM trisodium citrate at pH 7.0) in the absence or presence of complex **4**. (Inset: Enlargement of the circled area.) The arrows show the changes upon addition of increasing amounts of the complex. (B and C) UV-vis spectra of DMSO solutions of complex (B) **1** (0.1 mM) and (C) **4** (0.1 mM) in the presence of increasing amounts of CT DNA (*r*′ = [DNA]/[compound] = 0 to 0.8). The arrows show the changes upon addition of increasing amounts of CT DNA.

Published on 11 January 2018. Downloaded by National Library of Serbia on 5/30/2020 12:11:45 PM.

Table 4 UV-vis spectral features of the interaction of complexes **1–4** with CT DNA. UV-band (λ in nm) (percentage of the observed hyper-/hypo-chromism ($\Delta A/A_0$, %), blue-/red-shift of the λ_{max} ($\Delta\lambda$, nm)) and DNA-binding constants (K_b)

Compound	Band ($\Delta A/A_0$,[a] $\Delta\lambda$[b])	K_b (M^{-1})
Hindo[17]	314 (sh) (−10, 0)	$3.37(\pm0.23) \times 10^5$
Hmef[28]	324 (+10, 0)	$1.05(\pm0.02) \times 10^5$
1	321 (−7, 0)	$2.85(\pm0.17) \times 10^5$
2	296 (>+40, +12); 350 (−50, elm[c])	$3.69(\pm0.40) \times 10^5$
3	321 (−3, 0)	$3.24(\pm0.22) \times 10^4$
4	282 (+20, +15); 349 (−50, elm)[b,c]	$3.15(\pm0.12) \times 10^5$

[a] "+" denotes hyperchromism, "–" denotes hypochromism. [b] "+" denotes red-shift, "–" denotes blue-shift. [c] "elm" = eliminated.

DNA-binders than those bearing indomethacin ligands (**1** and **3**), with complex **2** having the highest K_b constant ($3.69(\pm0.40) \times 10^5$ M^{-1}) among the complexes. The K_b constants of complexes **1–4** are within the range found for other metal–NSAID complexes.[17,22,29–33,65–69] Further, the K_b constants are similar to or higher than that of the classical intercalator EB (1.23×10^5 M^{-1}) as calculated by Dimitrakopoulou *et al.*[78]

The interaction of complexes **1–4** with CT DNA was also monitored *via* DNA-viscosity measurements in the presence of increasing amounts of the complexes. As is known, the relative DNA-viscosity (η/η_0) is sensitive to relative DNA-length changes (L/L_0) occurring in the presence of a DNA-binder because they are correlated by the equation $L/L_0 = (\eta/\eta_0)^{1/3}$.[79] In the case of intercalation, the DNA-viscosity will increase, while in the case of non-classical intercalation, *i.e.* groove-binding or electrostatic interaction, the DNA-viscosity may decrease slightly or remain unchanged.

The changes in the viscosity of a CT DNA solution (0.1 mM) were studied in the presence of increasing amounts of complexes **1–4** (up to the value of $r = 0.35$). For all complexes, the DNA-viscosity showed a considerable increase upon their addition (Fig. 8). This increase may be attributed to intercalation of the complexes between DNA-bases because in the case of intercalation, the separation distance of the DNA bases will increase in order to accommodate the intercalating compounds and, subsequently, the DNA-viscosity will increase.[79] The existing conclusion of intercalation may clarify and enforce the preliminary conclusions derived from the UV-vis spectroscopic studies.

EB is a typical DNA-intercalator; its intercalation between DNA-bases *via* its planar phenanthridine ring results in the formation of the EB–DNA conjugate, which exhibits an intense fluorescence emission band at 592 nm with $\lambda_{ex} = 540$ nm. The displacement of EB from the EB–DNA conjugate induced by a compound that can intercalate DNA may indirectly verify the intercalating ability of the compound. In such a case, quenching of the EB–DNA fluorescence emission band will appear upon addition of the DNA-intercalating compound.[51,55a]

The EB–DNA conjugate was completely formed after pre-treatment of EB ([EB] = 20 μM) and DNA ([DNA] = 26 μM) for 1 h in buffer solution. The fluorescence emission spectra of the EB–DNA conjugate were recorded for increasing amounts of the

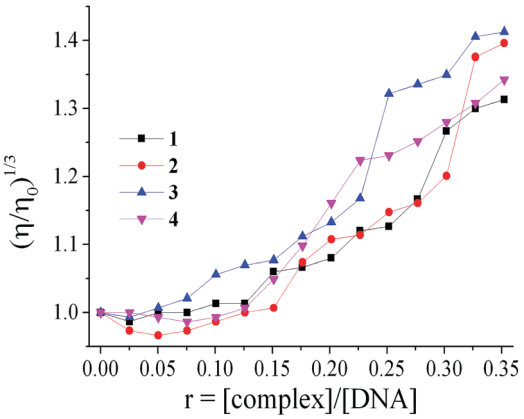

Fig. 8 Relative viscosity $(\eta/\eta_0)^{1/3}$ of CT DNA (0.1 mM) in buffer solution (150 mM NaCl and 15 mM trisodium citrate at pH 7.0) in the presence of increasing amounts of complexes **1–4** (r = [complex]/[DNA]).

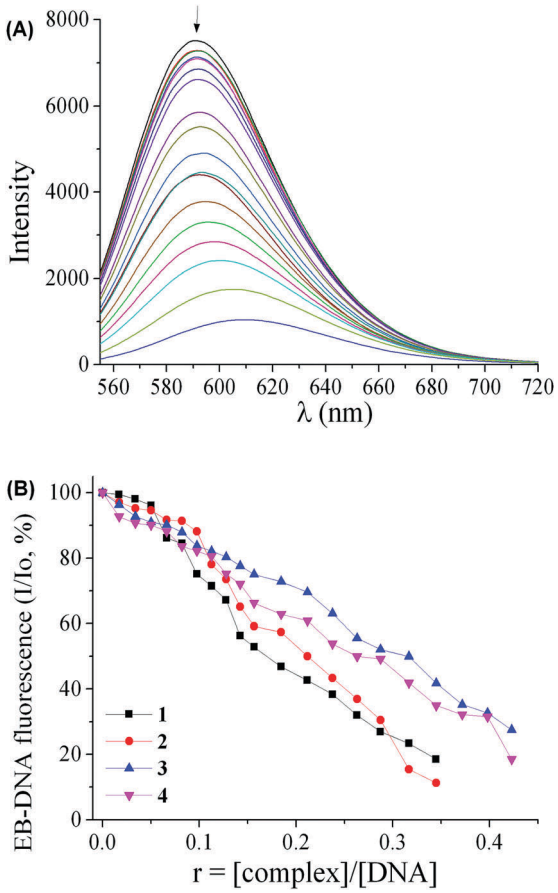

Fig. 9 (A) Fluorescence emission spectra ($\lambda_{exc} = 540$ nm) for EB–DNA ([EB] = 20 μM, [DNA] = 26 μM) in buffer solution in the absence and presence of increasing amounts of complex **2** (up to the value of $r = 0.35$). The arrow shows the changes of intensity upon increasing amounts of **2**. (B) Plot of the relative fluorescence intensity of EB–DNA ($\%I/I_0$) at $\lambda_{em} = 592$ nm *vs.* r (r = [complex]/[DNA]) in buffer solution (150 mM NaCl and 15 mM trisodium citrate at pH 7.0) in the presence of complexes **1–4** (quenching up to 18.5% of the initial EB–DNA fluorescence for **1**, 11.3% for **2**, 27.5% for **3** and 18.5% for **4**).

 This journal is © The Royal Society of Chemistry and the Centre National de la Recherche Scientifique 2018

Published on 11 January 2018. Downloaded by National Library of Serbia on 5/30/2020 12:11:45 PM.

Table 5 Percentage of EB–DNA fluorescence quenching ($\Delta I/I_0$, %), Stern–Volmer constants (K_{SV}) and quenching constants of EB–DNA fluorescence (k_q) for complexes **1–4**

Compound	$\Delta I/I_0$ (%)	K_{SV} (M^{-1})	k_q (M^{-1} s^{-1})
Hindo[22]	87.5	$3.62(\pm0.09) \times 10^5$	$1.57(\pm0.04) \times 10^{13}$
Hmef[30]	80.0	$1.58(\pm0.06) \times 10^5$	$6.87(\pm0.26) \times 10^{12}$
1	81.5	$8.96(\pm0.30) \times 10^4$	$3.90(\pm0.13) \times 10^{12}$
2	88.7	$7.71(\pm0.26) \times 10^4$	$3.35(\pm0.12) \times 10^{12}$
3	72.5	$3.75(\pm0.13) \times 10^4$	$1.63(\pm0.06) \times 10^{12}$
4	81.5	$6.67(\pm0.23) \times 10^4$	$2.90(\pm0.10) \times 10^{12}$

compounds (representatively shown for complex **2** in Fig. 9A up to r = 0.35). The complexes under study did not show any appreciable fluorescence emission bands at room temperature in solution or in the presence of EB or CT DNA under the same experimental conditions, *i.e.* with λ_{ex} = 540 nm. Therefore, the observed quenching upon addition of complexes **1–4** is significant (up to 88.7% of the initial EB–DNA fluorescence emission intensity, Table 5 and Fig. 9B) and can be attributed to the displacement of EB from the EB–DNA conjugate and its replacement by the complexes; thus, binding of the complexes at the DNA-intercalation sites may be indirectly concluded.[51]

The quenching of the EB–DNA fluorescence is in good agreement with the linear Stern–Volmer equation (eqn (S2), ESI†),[53] as shown in the corresponding Stern–Volmer plots ($R \sim 0.99$, Fig. S14, ESI†). The K_{SV} constants of the complexes (Table 5) are in the range reported for other metal–NSAID complexes,[17,22,29–33,65–69] with complex **1** having the highest K_{SV} constant among the complexes. The quenching constants of the compounds (k_q) in regard to their competition with EB were calculated according to eqn (S3) (ESI†), where the fluorescence lifetime of the EB–DNA system has the value τ_0 = 23 ns.[55b] The derived k_q constants (Table 5) are significantly higher than 10^{10} M^{-1} s^{-1}, suggesting that the quenching of the EB–DNA fluorescence by the complexes takes place *via* a static mechanism which leads to the formation of a new conjugate, obviously between DNA and each complex.[51]

Conclusions

The paper presented here showed that two chosen NSAIDs, HIndo and HMef, in the reaction with Ru(II)–arene complexes were bound monodentately *via* a carboxylate group. This was confirmed by NMR and IR spectroscopy results as well as by mass spectrometry.

Cytotoxicity studies revealed that the NSAIDs ligand Hindo, despite having poor activity itself, when coordinated to ruthenium(II)–arenes such as **1** and **3**, enhanced the cytotoxicity of the resulting complexes; meanwhile, the π-bonded arenes *p*-cymene (**1**) and toluene (**2**) did not seem to impact the *in vitro* cytotoxic potential of the complexes. A study of the mechanisms of action in CDDP resistant breast carcinoma MDA-MB-231 cells, using flow cytometry, revealed that complexes **1** and **3** arrested the cell cycle in S phase and caused rapid DNA-fragmentation and accumulation in sub-G1 phase. Even more than 40% of cells underwent either apoptotic or necrotic cell death after 24 h action of **1** and **3** at IC_{50}. Hindo certainly provided features that improved the cytotoxic activity of the resulting complexes **1** and **3**. Intercalation may be the most likely mode of interaction with DNA, as revealed by *in vitro* DNA-viscosity experiments with CT-DNA and EB-displacement experiments. The indomethacin-ruthenium complexes are better "DNA-binders" than the corresponding free indomethacin ligands. Additionally, fragmentation of DNA may be partially caused by indirect pathways, such as ROS production. Measurements of intracellular ROS production in MDA-MB-231 cells after 4 h of treatment with **1** and **3** at IC_{50} showed increased ROS levels, suggesting that the complexes exhibit multiple-layer cytotoxic effects that are also triggered by ROS release. The biological actions of most NSAIDs, including Hindo, customarily involve selective inhibition of cyclooxygenases (COX-1 and COX-2).[80,81] However, literature data provide evidence that the pharmacokinetic properties of NSAIDs may be also related to their ability to interact with membrane phospholipids and/or to disrupt membrane permeability, suggesting that effects at the cell membrane level may be an additional mechanism of action and toxicity of ruthenium-indomethacin complexes **1** and **3**.[82] In the present study, complexes **1–4** were also tested in regard to their ability to scavenge DPPH, ABTS and hydroxyl radicals, to inhibit soybean lipoxygenase activity and to bind to serum albumins. The results showed that, in general, the complexes are more active radical scavengers and LOX inhibitors than their corresponding free NSAIDs. The interaction of the complexes with albumins showed their potential ability to bind tightly and reversibly to albumins, enabling them to be transferred to and released at their potential biological targets.

In the expanding field of rational drug discovery, ruthenium complexes represent a promising class of small molecules that can be optimized to more specifically target tumour cells. The results of the present study of ruthenium(II)–arene complexes conjugated to indomethacin contribute to the development of so-called "combi-molecules" that may exhibit stronger or more specific antitumor effects than their single complexes or ligands alone. The present results may be considered to be promising for further biological studies and potential applications.

Abbreviations

K562	Human myelogenous leukemia cells
A549	Human lung adenocarcinoma cells
MDA-MB-231	Human breast adenocarcinoma cells
MRC-5	Non-tumor human lung fibroblast cells
MTT	3-(4,5-Dimethylthiazol-2-yl)-2,5-diphenyltetrazolium bromide dye
RPMI 1640	Roswell Park Memorial Institute nutrient medium (1640)
CDDP	*cis*-Diamminedichloridoplatinum(II), cisplatin
DCFH-DA	2′,7′-Dichlorodihydrofluorescein diacetate
DNA	Deoxyribonucleic acid

Published on 11 January 2018. Downloaded by National Library of Serbia on 5/30/2020 12:11:45 PM.

ROS	Reactive oxygen species
KP1019	Indazolium-*trans*-tetrachlorobis-(1*H*-indazole)ruthenate(III)
KP1339	Sodium-*trans*-tetrachlorobis-(1*H*-indazole)ruthenate(III)
NAMI	Sodium-*trans*-imidazoledimethylsulfoxidetetrachloro-ruthenate(III)
TrxR	Thioredoxin
NSAID	Non-steroidal anti-inflammatory drug
COX	Enzyme cyclooxygenase
Hindo	Indomethacin
Hmef	Mefenamic acid
DPPH	1,1-Diphenyl-picrylhydrazyl
$ABTS^{+\bullet}$	2,2′-Azinobis-(3-ethylbenzothiazoline-6-sulfonic acid) radicals
LOX	Soybean lipoxygenase
BSA	Bovine serum albumin
HSA	Human serum albumin
CT DNA	Calf-thymus deoxyribonucleic acid
UV-vis spectroscopy	Ultraviolet-visible spectroscopy
EB	Ethidium bromide
ABTS	2,2′-Azino-bis(3-ethylbenzothiazoline-6-sulphonic acid)
BHT	Butylated hydroxytoluene
Trolox	6-Hydroxy-2,5,7,8-tetramethylchromane-2-carboxylic acid
NDGA	Nordihydroguaiaretic acid
HEPES	4-(2-Hydroxyethyl)piperazine-1-ethanesulfonic acid
FCS	Fetal calf serum
DMSO	Dimethyl sulfoxide
PBS	Phosphate buffer solution
PI	Propidium iodide
RNaseA	Ribonuclease A
NDGA	4,4′-(2,3-Dimethylbutane-1,4-diyl)dibenzene-1,2-diol (nordihydroguaiaretic acid)
BHT	Butylated hydroxytoluene (2,6-di-*tert*-butyl-4-methylphenol)
EDTA	Ethylendiaminetetraacetic acid
SA	Serum albumin

Conflicts of interest

The authors declare no conflict of interest.

Acknowledgements

This work was supported by the grant from the Ministry of Education, Science and Technological Development of the Republic of Serbia, Grant numbers III 41026 and OI 172035. This research was also financed (*via* a scholarship to C. K.) by the General Secretariat for Research and Technology (GSRT) and Hellenic Foundation for Research and Innovation (HFRI), Greek Ministry of Education, Research and Religion.

References

1 B. Rosenberg, L. Van Camp and T. Krigas, Inhibition of cell division in *Escherichia coli* by electrolysis products from a platinum electrode, *Nature*, 1965, **205**, 698–699.
2 M. Mojic, A. Savic, V. B. Arion, M. Bulatovic, J. M. Poljarevic, Dj. Miljkovic, T. J. Sabo, S. Mijatovic, D. Maksimovic-Ivanic and S. Grguric-Sipka, Synthesis, X-ray structure and strong *in vitro* cytotoxicity of novel organoruthenium complexes, *J. Organomet. Chem.*, 2014, **749**, 142–149.
3 J.-F. Kou, C. Qian, J.-Q. Wang, X. Chen, L.-L. Wang, H. Cha and L.-N. Ji, Chiral ruthenium(II) anthraquinone complexes as dual inhibitors of topoisomerases I and II, *J. Biol. Inorg. Chem.*, 2012, **17**, 81–96.
4 Z. Luo, L. Yu, F. Yang, Z. Zhao, B. Yu, H. Lai, K.-H. Wong, S.-M. Ngai, W. Zheng and T. Chen, Ruthenium polypyridyl complexes as inducer of ROS-mediated apoptosis in cancer cells by targeting thioredoxin reductase, *Metallomics*, 2014, **6**, 1480–1490.
5 F. Li, J. G. Collins and F. R. Keene, Ruthenium complexes as antimicrobial agents, *Chem. Soc. Rev.*, 2015, **44**, 2529–2542.
6 H. Song, J. T. Kaiser and J. K. Barton, Crystal structure of Δ-$[Ru(bpy)_2dppz]^{2+}$ bound to mismatched DNA reveals side-by-side metalloinsertion and intercalation, *Nat. Chem.*, 2012, **4**, 615–620.
7 A. Levina, A. Mitra and P. A. Lay, Recent developments in ruthenium anticancer drugs, *Metallomics*, 2009, **1**, 458–470.
8 A. R. Delgado, A. Galdamez, J. Villena, G. P. Reveco and A. F. Thomet, Synthesis, characterization and *in vitro* biological evaluation of $[Ru(\eta^6\text{-arene})(N,N)Cl]PF_6$ compounds using the natural products arenes methylisoeugenol and anethole, *J. Organomet. Chem.*, 2015, **782**, 131–137.
9 R. Gogna, E. Madan, B. K. Keppler and U. Pati, Gallium compound GaQ_3-induced Ca^{2+} signalling triggers p53-dependent and -independent apoptosis in cancer cells, *Br. J. Pharmacol.*, 2012, **166**, 617–636.
10 L. Tabrizi and H. Chiniforoshan, Ruthenium(II) *p*-cymene complexes of naphthoquinone derivatives as antitumor agents: a structure–activity relationship study, *J. Organomet. Chem.*, 2016, **822**, 211–220.
11 K. S. Subran, S. Banjerjee, A. Mondal and P. Paira, Amberlite IR-120(H)-mediated ''on water'' synthesis of novel anti-cancer ruthenium(II)-*p*-cymene 2-pyridinylbenzothiazole (BTZ), 2-pyridinylbenzoxazole (BOZ) & 2-pyridinylbenzimidazole (BIZ) scaffolds, *New J. Chem.*, 2016, **40**, 10333–10334.
12 A. Savic, M. Dulovic, J. M. Poljarevic, S. Misirlic-Dencic, M. Jovanovic, A. Bogdanovic, V. Trajkovic, T. J. Sabo, S. Grguric-Sipka and I. Markovic, Synthesis and *in vitro* Anticancer Activity of Ruthenium-Cymene Complexes with Cyclohexyl-Functionalized Ethylenediamine-*N*,*N*′-diacetate-Type Ligands, *ChemMedChem*, 2011, **6**, 1884–1891.
13 N. V. Chandrasekharan, H. Dai, K. L. T. Roos, N. K. Evanson, J. Tomisik, T. S. Elton and D. L. Simmons, COX-3, a

 This journal is © The Royal Society of Chemistry and the Centre National de la Recherche Scientifique 2018

Published on 11 January 2018. Downloaded by National Library of Serbia on 5/30/2020 12:11:45 PM.

cyclooxygenase-1 variant inhibited by acetaminophen and other analgesic/antipyretic drugs: cloning, structure, and expression, *Proc. Natl. Acad. Sci. U. S. A.*, 2002, **99**, 13926–13931.

14 K. Y. Shamsudin, M. Kazemi, H. Gutieerrez-de-Terán and J. Aqvist, Origin of the Enigmatic Stepwise Tight-Binding Inhibition of Cyclooxygenase-1, *Adv. Biochem.*, 2015, **54**(49), 7283–7291.

15 K.-S. Kim, J.-H. Yoon, J. K. Kim, S. J. Baek, T. E. Eling, W. J. Lee, J. Ryu, J. G. Lee, J. Lee and J. Yoo, Cyclooxygenase inhibitors induce apoptosis in oral cavity cancer cells by increased expression of nonsteroidal anti-inflammatory drug-activated gene, *Biochem. Biophys. Res. Commun.*, 2004, **325**, 1298–1303.

16 D. H. Woo, I. Han and G. Jung, Mefenamic acid-induced apoptosis in human liver cancer cell-lines through caspase-3 pathway, *Life Sci.*, 2004, **75**, 2439–2449.

17 G. Psomas and D. P. Kessissoglou, Quinolones and non-steroidal anti-inflammatory drugs interacting with copper(II), nickel(II), cobalt(II) and zinc(II): structural features, biological evaluation and perspectives, *Dalton Trans.*, 2013, **42**, 6252–6276.

18 L. Tabrizi, H. Chiniforoshan, P. McArdle, M. Ebrahimi and T. Khayamian, A novel bioactive Cd(II) polymeric complex with mefenamic acid: synthesis, crystal structure and biological evaluations, *Inorg. Chim. Acta*, 2015, **432**, 176–184.

19 U. Weser, K. Sellinger, E. Lengfelder, W. Werner and J. Strahle, Structure of Cu_2(indomethacin)$_4$ and the reaction with superoxide in aprotic systems, *Biochim. Biophys. Acta*, 1980, **631**, 232–245.

20 J. E. Weder, T. W. Hambley, B. J. Kennedy, P. A. Lay, D. MacLachlan, R. Bramley, C. D. Delfs, K. S. Murray, B. Moubaraki, B. Warwick, J. R. Biffin and H. L. Regtop, Anti-Inflammatory Dinuclear Copper(II) Complexes with Indomethacin. Synthesis, Magnetism and EPR Spectroscopy. Crystal Structure of the *N*,*N*-Dimethylformamide Adduct, *Inorg. Chem.*, 1999, **38**, 1736–1744.

21 Y. R. Morgan, P. Turner, B. J. Kennedy, T. W. Hambley, P. A. Lay, J. R. Biffin, H. L. Regtop and B. Warwick, Preparation and characterization of dinuclear copper-indomethacin anti-inflammatory drugs, *Inorg. Chim. Acta*, 2001, **324**, 150–161.

22 A. Tarushi, C. P. Raptopoulou, V. Psycharis, D. P. Kessissoglou, A. N. Papadopoulos and G. Psomas, Structure and biological perspectives of Cu(II)-indomethacin complexes, *J. Inorg. Biochem.*, 2014, **140**, 185–198.

23 A. Galani, D. Kovala-Demertzi, N. Kourkoumelis, A. Koutsodimou, V. Dokorou, Z. Ciunik, U. Russo and M. A. Demertzi, Organotin adducts of indomethacin: synthesis, crystal structures and spectral characterization of the first organotin complexes of indomethacin, *Polyhedron*, 2004, **23**, 2021–2030.

24 J. E. F. Reynolds and W. Martindale, *The Extra Pharmacopoeia*, The Pharmaceutical Press, London, 31st edn, 1996.

25 D. M. Boothe in *Veterinary Pharmacology and Therapeutics*, ed. H. R. Adams, Iowa State University Press, Ames, IA, 8th edn, 2001, pp. 433–435.

26 S. Lorinc, M. Koman, M. Melnik, J. Moncol and D. Ondrusova, Bis(flufenamato-κO)bis(3-pyridylmethanol-κ^2N,O)copper(II), *Acta Crystallogr.*, 2004, **60**, m590–m592.

27 G. Facchin, M. H. Torre and E. J. Baran, Crystal Structure and Spectroscopic Behaviour of a Binuclear Copper(II) Complex of Mefenamic Acid and Dimethylsulfoxide, *Z. Naturforsch., B: J. Chem. Sci.*, 1998, **53**, 871–874.

28 R. P. Sharma, S. Kumar, P. Venugopalan, V. Ferretti, A. Tarushi, G. Psomas and M. Witwicki, New copper(II) complexes of the anti-inflammatory drug mefenamic acid: a concerted study including synthesis, physicochemical characterization and their biological evaluation, *RSC Adv.*, 2016, **6**, 88546–88558.

29 F. Dimiza, S. Fountoulaki, A. N. Papadopoulos, C. A. Kontogiorgis, V. Tangoulis, C. P. Raptopoulou, V. Psycharis, A. Terzis, D. P. Kessissoglou and G. Psomas, Non-steroidal antiinflammatory drug–copper(II) complexes: structure and biological perspectives, *Dalton Trans.*, 2011, **40**, 8555–8568.

30 F. Dimiza, A. N. Papadopoulos, V. Tangoulis, V. Psycharis, C. P. Raptopoulou, D. P. Kessissoglou and G. Psomas, Biological evaluation of non-steroidal anti-inflammatory drugs–cobalt(II) complexes, *Dalton Trans.*, 2010, **39**, 4517–4528.

31 S. Tsiliou, L. A. Kefala, A. G. Hatzidimitriou, D. P. Kessissoglou, F. Perdih, A. N. Papadopoulos, I. Turel and G. Psomas, Cobalt(II) complexes with non-steroidal anti-inflammatory drugs and α-diimines, *J. Inorg. Biochem.*, 2016, **160**, 125–139.

32 X. Totta, A. A. Papadopoulou, A. G. Hatzidimitriou, A. Papadopoulos and G. Psomas, Synthesis, structure and biological activity of nickel(II) complexes with mefenamato and nitrogen-donor ligands, *J. Inorg. Biochem.*, 2015, **145**, 79–93.

33 A. Tarushi, Z. Karaflou, J. Kljun, I. Turel, G. Psomas, A. N. Papadopoulos and D. P. Kessissoglou, Antioxidant capacity and DNA-interaction studies of zinc complexes with a non-steroidal anti-inflammatory drug, mefenamic acid, *J. Inorg. Biochem.*, 2013, **128**, 85–96.

34 J. Feng, X. Du, H. Liu, X. Sui, C. Zhang, Y. Tang and J. Zhang, Manganese-mefenamic acid complexes exhibit high lipoxygenase inhibitory activity, *Dalton Trans.*, 2014, **43**, 10930–10939.

35 V. Dokorou, Z. Ciunik, U. Russo and D. Kovala-Demertzi, Synthesis, crystal structures and spectroscopic studies of diorganotin derivatives with mefenamic acid. Crystal and molecular structures of 1,2:3,4-di-μ_2-2-[(2,3-dimethylphenyl)-amino]-benzoato-*O*,*O*-1,3-bis-2-[(2,3-dimethylphenyl)amino]-benzoato-*O*-1,2,4:2,3,4-di-μ_3-oxo-tetrakis[di-methyltin(IV)] and 1,2:3,4-di-μ_2-2-[(2,3-dimethylphenyl)amino]-benzoato-*O*,*O*-1,3-bis-2-[(2,3-dimethylphenyl)amino]benzoato-*O*-1,2,4:2,3,4-di-μ_3-oxo-tetrakis[di-*n*-butyltin(IV)], *J. Organomet. Chem.*, 2001, **630**, 205–214.

36 F. Aman, M. Hanif, W. A. Siddiqui, A. Ashraf, L. K. Filak, J. Reynisson, T. Söhnel, S. M. F. Jamieson and C. G. Hartinger, Anticancer Ruthenium(η^6-*p*-cymene) Complexes of Nonsteroidal Anti-inflammatory Drug Derivatives, *Organometallics*, 2014, **33**, 5546–5553.

37 E. Paunescu, S. McArthur, M. Soudani, R. Scopelliti and P. J. Dyson, Nonsteroidal Anti-inflammatory – Organometallic Anticancer Compounds, *Inorg. Chem.*, 2016, **55**, 1788–1808.

Published on 11 January 2018. Downloaded by National Library of Serbia on 5/30/2020 12:11:45 PM.

38 A. Ashraf, M. Hanif, M. Kubanik, T. Söhnel, S. M. F. Jamieson, A. Bhattacharyya and C. G. Hartinger, Aspirin-inspired organometallic compounds: structural characterization and cytotoxicity, *J. Organomet. Chem.*, 2017, **839**, 31–37.

39 F. Aman, M. Hanif, M. Kubanik, A. Ashraf, T. Schnel, S. M. F. Jamieson, W. A. Siddiqui and C. G. Hartinger, Anti-Inflammatory Oxicams as Multi-donor Ligand Systems: pH- and Solvent Dependent Coordination Modes of Meloxicam and Piroxicam to Ru and Os, *Chem. – Eur. J.*, 2017, **23**, 1–11.

40 S. B. Jensen, S. J. Rodger and M. D. Spicer, Facile preparation of η^6-*p*-cymene ruthenium diphosphine complexes. Crystal structure of $[(\eta^6\text{-}p\text{-cymene})Ru(dppf)Cl]PF_6$, *J. Organomet. Chem.*, 1998, **556**, 151–158.

41 R. A. Zelonka and M. C. Baird, Benzene Complexes of Ruthenium(II), *Can. J. Chem.*, 1972, **50**, 3063–3072.

42 J. Marmur, A Procedure for the Isolation of Deoxyribonucleic Acid from Micro-organisms, *J. Mol. Biol.*, 1961, **3**, 208–218.

43 M. F. Reichmann, S. A. Rice, C. A. Thomas and P. Doty, A Further Examination of the Molecular Weight and Size of Desoxypentose Nucleic Acid, *J. Am. Chem. Soc.*, 1954, **76**, 3047–3053.

44 B. Rosenberg, L. Van Camp, J. E. Trosco and V. H. Mansour, Platinum compounds: a new class of potent antitumour agents, *Nature*, 1969, **222**, 385–386.

45 R. Supino, Methods in Molecular Biology, in *In Vitro Toxicity Testing Protocols*, ed. S. O'Hare and C. K. Atterwill, Humana Press, New Jersey, 1995, vol. 43, pp. 137–149.

46 M. Patra, T. Joshi, V. Pierroz, K. Ingram, M. Kaiser, S. Ferrari, B. Spingler, J. Keiser and G. Gasser, DMSO-Mediated Ligand Dissociation: Renaissance for Biological Activity of N-Heterocyclic $[Ru(\eta^6\text{-arene})Cl_2]$ Drug Candidates, *Chem. – Eur. J.*, 2013, **19**, 14768–14772.

47 M. G. Ormerod, Analysis of DNA-General Methods, in *Flow Cytometry, a Practical Approach*, ed. M. G. Ormerod, Oxford University Press, New York, 1994, pp. 119–125.

48 E. Eruslanov and S. Kusmartsev, Identification of ROS using oxidized DCFDA and flow-cytometry, *Methods Mol. Biol.*, 2010, **594**, 57–72.

49 (*a*) C. Kontogiorgis and D. Hadjipavlou-Litina, Biological Evaluation of Several Coumarin Derivatives Designed as Possible Anti-inflammatory/Antioxidant Agents, *J. Enzyme Inhib. Med. Chem.*, 2003, **18**, 63–69; (*b*) R. Cini, G. Giorgi, A. Cinquantini, C. Rossi and M. Sabat, Metal complexes of the antiinflammatory drug piroxicam, *Inorg. Chem.*, 1990, **29**, 5197–5200.

50 T. Nash, The Colorimetric Estimation of Formaldehyde by Means of the Hantzsch Reaction, *Biochem. J.*, 1953, **55**, 416–421.

51 J. R. Lakowicz, *Principles of Fluorescence Spectroscopy*, Plenum Press, New York, 3rd edn, 2006.

52 L. Stella, A. L. Capodilupo and M. Bietti, A reassessment of the association between azulene and [60]fullerene. Possible pitfalls in the determination of binding constants through fluorescence spectroscopy, *Chem. Commun.*, 2008, 4744–4746.

53 (*a*) Y. Wang, H. Zhang, G. Zhang, W. Tao and S. Tang, Interaction of the flavonoid hesperidin with bovine serum albumin: a fluorescence quenching study, *J. Lumin.*, 2007, **126**, 211–218; (*b*) G. Zhao, H. Lin, S. Zhu, H. Sun and Y. Chen, Dinuclear palladium(II) complexes containing two monofunctional [Pd(en)(pyridine)Cl] units bridged by Se or S. Synthesis, characterization, cytotoxicity and kinetic studies of DNA-binding, *J. Inorg. Biochem.*, 1998, **70**, 219–226; (*c*) V. Rajendiran, R. Karthik, M. Palaniandavar, H. Stoeckli-Evans, V. S. Periasamy, M. A. Akbarsha, B. S. Srinag and H. Krishnamurthy, Mixed-Ligand Copper(II)-phenolate Complexes: Effect of Coligand on Enhanced DNA and Protein Binding, DNA Cleavage, and Anticancer Activity, *Inorg. Chem.*, 2007, **46**, 8208–8221.

54 (*a*) A. Wolfe, G. Shimer and T. Meehan, Polycyclic aromatic hydrocarbons physically intercalate into duplex regions of denatured DNA, *Biochemistry*, 1987, **26**, 6392–6396; (*b*) G. Pratviel, J. Bernadou and B. Meunier, DNA and RNA Cleavage by Metal Complexes, *Adv. Inorg. Chem.*, 1998, **45**, 251–262.

55 (*a*) W. D. Wilson, L. Ratmeyer, M. Zhao, L. Strekowski and D. Boykin, The search for structure-specific nucleic acid-interactive drugs: effects of compound structure on RNA versus DNA interaction strength, *Biochemistry*, 1993, **32**, 4098–4104; (*b*) D. P. Heller and C. L. Greenstock, Fluorescence lifetime analysis of DNA intercalated ethidium bromide and quenching by free dye, *Biophys. Chem.*, 1994, **50**, 305–312.

56 X. Huang, H. D. Halicka, F. Traganos, T. Tanaka, A. Kurose and Z. Darzynkiewicz, Cytometric assessment of DNA damage in relation to cell cycle phase and apoptosis, *Cell Proliferation*, 2005, **38**, 223–243.

57 S. Nikolić, D. M. Opsenica, V. Filipović, B. Dojčinović, S. Aranđelović, S. Radulović and S. Grgurić-Šipka, Strong *in Vitro* Cytotoxic Potential of New Ruthenium–Cymene Complexes, *Organometallics*, 2015, **34**, 3464–3473.

58 F. P. Intini, J. Zajac, V. Novohradsky, T. Saltarella, C. Pacifico, V. Brabec, G. Natile and J. Kasparkova, Novel Antitumor Platinum(II) Conjugates Containing the Nonsteroidal Anti-inflammatory Agent Diclofenac: Synthesis and Dual Mechanisms of Antiproliferative Effects, *Inorg. Chem.*, 2017, **56**, 1483–1497.

59 D. Plano, D. N. Karelia, M. K. Pandey, J. E. Spallholz, S. Amin and A. K. Sharma, Design, Synthesis, and Biological Evaluation of Novel Selenium (Se-NSAID) Molecules as Anticancer Agents, *J. Med. Chem.*, 2016, **59**, 1946–1959.

60 A. W. Leung, T. de Silva, M. B. Bally and W. W. Lockwood, Cancer Synthetic lethality in lung cancer and translation to clinical therapies, *Mol. Cancer*, 2016, **15**, 61–77.

61 H. Raza and A. John, Implications of altered glutathione metabolism in aspirin-induced oxidative stress and mitochondrial dysfunction in HepG2 cells, *PLoS One*, 2012, **7**, e36325.

62 S. Kobayashi, S. Okada, H. Yoshida and S. Fujimura, Indomethacin enhances the cytotoxicity of VCR and ADR in human pulmonary adenocarcinoma cells, *Tohoku J. Exp. Med.*, 1997, **181**, 361–370.

63 C. P. Duffy, C. J. Elliott, R. A. O' Connor, M. M. Heenan, S. Coyle, I. M. Cleary, K. Kavanagh, S. Verhaegen,

 This journal is © The Royal Society of Chemistry and the Centre National de la Recherche Scientifique 2018

Published on 11 January 2018. Downloaded by National Library of Serbia on 5/30/2020 12:11:45 PM.

C. M. O'Loughlin, R. NicAmhlaoibh and M. Clynes, Enhancement of chemotherapeutic drug toxicity to human tumour cells *in vitro* by a subset of non-steroidal anti-inflammatory drugs (NSAIDs), *Eur. J. Cancer*, 1998, **34**, 1250–1259.

64 R. N. Young, Inhibitors of 5-lipoxygenase: a therapeutic potential yet to be fully realized?, *Eur. J. Med. Chem.*, 1999, **34**, 671–685.

65 A. Tarushi, C. Kakoulidou, C. P. Raptopoulou, V. Psycharis, D. P. Kessissoglou, I. Zoi, A. N. Papadopoulos and G. Psomas, Zinc complexes of diflunisal: synthesis, characterization, structure, antioxidant activity, and *in vitro* and *in silico* study of the interaction with DNA and albumins, *J. Inorg. Biochem.*, 2017, **170**, 85–97.

66 A. Tarushi, P. Kastanias, C. P. Raptopoulou, V. Psycharis, D. P. Kessissoglou, A. N. Papadopoulos and G. Psomas, Zinc complexes of flufenamic acid: characterization and biological evaluation, *J. Inorg. Biochem.*, 2016, **163**, 332–345.

67 S. Perontsis, A. G. Hatzidimitriou, A. N. Papadopoulos and G. Psomas, Nickel-diflunisal complexes: synthesis, characterization, *in vitro* antioxidant activity and interaction with DNA and albumins, *J. Inorg. Biochem.*, 2016, **162**, 9–21.

68 M. Zampakou, A. G. Hatzidimitriou, A. N. Papadopoulos and G. Psomas, Neutral and cationic manganese(II)–diclofenac complexes: structure and biological evaluation, *J. Coord. Chem.*, 2015, **68**, 4355–4372.

69 M. Zampakou, N. Rizeq, V. Tangoulis, A. N. Papadopoulos, F. Perdih, I. Turel and G. Psomas, Manganese(II) Complexes with the Non-steroidal Anti-Inflammatory Drug Tolfenamic Acid: Structure and Biological Perspectives, *Inorg. Chem.*, 2014, **53**, 2040–2052.

70 K. C. Skyrianou, F. Perdih, A. N. Papadopoulos, I. Turel, D. P. Kessissoglou and G. Psomas, Nickel–quinolones interaction part 5-biological evaluation of nickel(II) complexes with first-, second- and third-generation quinolones, *J. Inorg. Biochem.*, 2011, **105**, 1273–1285.

71 Z. Liu, B. Wang, Z. Yang, Y. Li, D. Qin and T. Li, Synthesis, crystal structure, DNA interaction and antioxidant activities of two novel water-soluble Cu(2+) complexes derivated from 2-oxo-quinoline-3-carbaldehyde Schiff-bases, *Eur. J. Med. Chem.*, 2009, **44**, 4477–4484.

72 E. Pontiki and D. Hadjipavlou-Litina, Synthesis and pharmacochemical evaluation of novel aryl-acetic acid inhibitors of lipoxygenase, antioxidants, and anti-inflammatory agents, *Bioorg. Med. Chem.*, 2007, **15**, 5819–5827.

73 C. Tan, J. Liu, H. Li, W. Zheng, S. Shi, L. Chen and L. Ji, Differences in structure, physiological stability, electrochemistry, cytotoxicity, DNA and protein binding properties between two Ru(III) complexes, *J. Inorg. Biochem.*, 2008, **102**, 347–358.

74 O. H. Laitinen, V. P. Hytonen, H. R. Nordlund and M. S. Kulomaa, Genetically engineered avidins and streptavidins, *Cell. Mol. Life Sci.*, 2006, **63**, 2992–3017.

75 (*a*) B. M. Zeglis, V. C. Pierre and J. K. Barton, Metallo-intercalators and metallo-insertors, *Chem. Commun.*, 2007, 4565–4579; (*b*) C. N. Banti and S. K. Hadjikakou, Non-Steroidal Anti-Inflammatory Drugs (NSAIDs) in Metal Complexes and Their Effect at the Cellular Level, *Eur. J. Inorg. Chem.*, 2016, 3048–3071.

76 Q.-L. Zhang, J.-G. Liu, H. Chao, G.-Q. Xue and L.-N. Ji, DNA-binding and photocleavage studies of cobalt(III) polypyridyl complexes: $[Co(phen)_2IP]^{3+}$ and $[Co(phen)_2PIP]^3$, *J. Inorg. Biochem.*, 2001, **83**, 49–55.

77 A. M. Pyle, J. P. Rehmann, R. Meshoyrer, C. V. Kumar, N. J. Turro and J. K. Barton, Mixed-ligand complexes of ruthenium(II): factors governing binding to DNA, *J. Am. Chem. Soc.*, 1989, **111**, 3051–3058.

78 A. Dimitrakopoulou, C. Dendrinou-Samara, A. A. Pantazaki, M. Alexiou, E. Nordlander and D. P. Kessissoglou, Synthesis, structure and interactions with DNA of novel tetranuclear, $[Mn_4(II/II/II/IV)]$ mixed valence complexes, *J. Inorg. Biochem.*, 2008, **102**, 618–628.

79 J. L. Garcia-Gimenez, M. Gonzalez-Alvarez, M. Liu-Gonzalez, B. Macias, J. Borras and G. Alzuet, Toward the development of metal-based synthetic nucleases: DNA binding and oxidative DNA cleavage of a mixed copper(II) complex with *N*-(9*H*-purin-6-yl)benzenesulfonamide and 1,10-phenantroline. Antitumor activity in human Caco-2 cells and Jurkat T lymphocytes. Evaluation of p53 and Bcl-2 proteins in the apoptotic mechanism, *J. Inorg. Biochem.*, 2009, **103**, 923–934.

80 P. P. Rao, S. N. Kabir and T. Mohamed, Nonsteroidal Anti-Inflammatory Drugs (NSAIDs): Progress in Small Molecule Drug Development, *Pharmaceuticals*, 2010, **3**, 1530–1549.

81 M. G. Perrone, A. Scilimati, L. Simone and P. Vitale, Selective COX-1 inhibition: a therapeutic target to be reconsidered, *Curr. Med. Chem.*, 2010, **17**, 3769–3805.

82 C. Pereira-Leite, C. Nunes and S. Reis, Interaction of non-steroidal anti-inflammatory drugs with membranes: *in vitro* assessment and relevance for their biological actions, *Prog. Lipid Res.*, 2013, **52**, 571–584.